THE ASTROPHYSICAL JOURNAL, 436:152–175, 1994 November 20

A HIGH-RESOLUTION SURVEY OF INTERSTELLAR Na I D_1 LINES

DANIEL E. WELTY[1]
University of Chicago, Astronomy and Astrophysics Center, 5640 S. Ellis Avenue, Chicago, IL 60637
L. M. HOBBS[1]
University of Chicago, Yerkes Observatory, Williams Bay, WI 53191-0258
AND
VARSHA P. KULKARNI[2]
University of Chicago, Astronomy and Astrophysics Center, 5640 S. Ellis Avenue, Chicago, IL 60637
Received 1994 February 22; accepted 1994 May 20

ABSTRACT

We present high-resolution (0.5 km s^{-1}) spectra, obtained with the McDonald Observatory 2.7 m coudé echelle spectrograph, of interstellar Na I D_1 absorption toward 38 bright stars. Numerous narrow, closely blended absorption components, showing resolved Na I hyperfine structure, are evident in these spectra; such narrow components appear in both low halo and quite local gas, as well as in gas toward more distant disk stars. We have used the method of profile fitting in an attempt to determine column densities, line widths, and velocities for the individual interstellar clouds contributing to the observed absorption lines. The resulting sample of 276 clouds is significantly larger, and likely more complete, than several previous samples of "individual" interstellar clouds, and allows more precise investigation of various statistical properties. We find that the cloud column density (N) and line width parameter (b) are not correlated, for 0.3 km $s^{-1} \lesssim b \lesssim 1.5$ km s^{-1} and 10.0 $cm^{-2} \lesssim \log [N(\text{Na I})] \lesssim 11.6$ cm^{-2}. The median b is about 0.73 km s^{-1}, the median log N is about 11.09 cm^{-2}, and the median separation between adjacent components is about 2.0 km s^{-1}. All these are overestimates of the true median values, however, due to our inability to completely resolve all the component structure present in some cases; even at a resolution of 0.5 km s^{-1}, we may have discerned only 60% of the full number of individual components actually present. The one-dimensional dispersion of component velocities, in the local standard of rest, is approximately 8.6 km s^{-1}; the distribution of velocities is broader and displaced to more negative velocities for the weaker components. If 80 K is a representative temperature for the interstellar clouds seen in Na I absorption, then at least 38% (and probably the majority) of the clouds have subsonic internal turbulent motions. The range in N(H I) observed at a given N(Na I) increases as N(Na I) decreases below about 10^{11} cm^{-2}, so that N(Na I) becomes a less reliable predictor of N(H I) at low column densities. These spectra will be quite useful in future detailed studies of these lines of sight with the *HST* GHRS echelle—to determine accurate velocities and to reveal the detailed interstellar component structures that cannot be discerned at the 3.5 km s^{-1} resolution available with the GHRS.

Subject headings: ISM: abundances — ISM: atoms — ISM: kinematics and dynamics — line: profiles

1. INTRODUCTION

The initial results from a new survey of the interstellar Na I D_1 line in the spectra of 38 bright stars were described previously (Hobbs & Welty 1991, hereafter Paper I). The primary feature of the survey is that it employs the high spectral resolving power $R = \lambda/\Delta\lambda = 6 \times 10^5$, corresponding to wavelength and velocity resolutions (FWHM) of $\Delta\lambda = 10$ mÅ and $\Delta v = 0.5$ km s^{-1} at the D_1 line. For sufficiently narrow, unblended interstellar lines, this instrumental resolution is sufficient to distinguish the two s-resolved hyperfine-structure (hfs) components of either Na I D line, each of which is split by about 1.05 km s^{-1} (McNutt & Mack 1963). More precisely, the hfs components formed in an individual interstellar cloud characterized by a line width parameter $b = (2kT/m + 2v_t^2)^{1/2} \leq 0.6$ km s^{-1} will be partially resolved at this resolution (Hobbs 1969b). Such narrow lines can arise in gas which satisfies simultaneously the limits $T \leq 300$ K and $v_t \leq 0.3$ km s^{-1}, for example, where v_t is the one-dimensional rms value of a Gaussian spectrum of internal "turbulent" velocities. These limits probably are satisfied in many diffuse interstellar clouds (Spitzer 1978). Hence, at adequate instrumental resolution, resolved Na I hfs components should appear widely as an immediate, uniquely recognizable signature of cold gas, apart from the obscuring effects of any overlapping lines which might arise in physically separate clouds with similar radial velocities along a given line of sight.

The first successful observations of resolved hfs components of interstellar D lines were achieved with a Michelson interferometer ($R \sim 6 \times 10^5$) by Blades, Wynne-Jones, & Wayte (1980), in four clouds along the light paths to δ Cyg and α Cyg. Observations of SN 1987A obtained near its maximum brightness by Pettini (1988), also at $R \sim 6 \times 10^5$, showed resolved Na I hfs components in several interstellar clouds along that line of sight. In Paper I, we presented the results of more extensive observations at the D_1 line of 43 kinematically distinct clouds in the directions of six of the 38 stars in our survey, along with an analysis of the measured line widths. The absorption lines arising in 13 of the 43 clouds were seen to be sufficiently narrow and unblended to reveal resolved hfs components; an additional 13 clouds showed comparably narrow, but more strongly blended, hfs components. The results pre-

[1] Guest Observer, McDonald Observatory, University of Texas.
[2] Current address: Space Telescope Science Institute, 3700 San Martin Drive, Baltimore, MD 21218.

sented in Paper I thus suggest that such narrow lines are common; limits on T and v_t further suggest that the three-dimensional turbulent velocity $(3)^{1/2} \times v_t$ is often subsonic if $T \sim 80$ K.

The present paper describes the results of the complete observing program for our 38 program stars. The primary goals of the work are to discern the individual interstellar absorption components along the chosen lines of sight and to obtain stringent, rigorous upper limits on the temperatures and the internal mass motions for the resulting relatively large sample of individual diffuse clouds. Such limits have hitherto been particularly difficult to obtain for most single interstellar clouds. As will be apparent, these very high resolution spectra exhibit numerous narrow, closely blended components that were not distinguished even at a resolution of 1 km s^{-1} (e.g., Hobbs 1969a). These spectra will be quite useful for intensive studies of these lines of sight using lower resolution UV data obtained, for example, with the *Hubble Space Telescope*/Goddard High Resolution Spectrograph (*HST*/GHRS). While we have probably not resolved all the component structure present in some of the lines of sight, our sample of 276 interstellar clouds allows more detailed investigation of the distribution of individual cloud column densities, line widths, and velocities than has previously been possible.

In §§ 2 and 3, we present a more complete discussion of the observations, data reduction, and data analysis than was given for the small preliminary sample presented in Paper I. In §§ 4 and 5, we discuss the implications of these new high-resolution data for our understanding of various statistical properties of the interstellar clouds, of the relationship between Na I and H I column densities, and of the physical conditions along some of the specific lines of sight in the survey. In Appendices A and B, we give detailed derivations of the oscillator strengths appropriate for the individual *s*-resolved hyperfine components of absorption lines due to Na I, K I, and ^{7}Li I and of the resulting absorption line profiles, respectively.

2. OBSERVATIONS AND DATA REDUCTION

2.1. *The Program Stars*

The stars included in this investigation were chosen both because they are apparently bright ($V \lesssim 4.5$ in most cases) and because the interstellar D_1 lines in their spectra were known (primarily from earlier interferometric observations; Hobbs 1969a) to show at least one component of intermediate strength, as it is generally difficult to determine reliable widths for line components which are either very weak or strongly saturated. The 38 stars observed are listed in Table 1. The Galactic longitude, Galactic latitude, visual magnitude, spectral type, color excess $E(B-V)$, and distance are given in successive columns for each star; the magnitudes of variable stars are given to only one decimal place. The entries listed for 32 stars are taken from Hobbs (1969a), where the sources of the various data were enumerated in some detail. The data for γ Cas, π^5 Ori, S Mon, o^2 CMa, τ CMa, and ϵ Ari A were taken from the same sources (Marschall & Hobbs 1973; Hobbs 1978a, b; Hobbs, Blitz, & Magnani 1986). These various stellar data have also been compiled independently for 18 of the stars by Shull & Van Steenberg (1985). A comparison of the values adopted for a particular star by the two groups may give an indication of the actual uncertainties in its spectral type and in the derived reddening and distance. For the immediate purposes of this study, highly accurate values of these stellar data are not needed, however.

TABLE 1

STELLAR DATA

Star	l (° ′)	b (° ′)	V	Type	E(B-V)	Distance (pc)
γ Cas	123 34	-02 09	2.4	B0.5 IVe	0.18	180
ϵ Ari A	158 42	-32 31	4.63	A2 V	0.00	70
17 Tau	166 10	-23 51	3.70	B6 III	0.02	125
η Tau	166 40	-23 28	2.87	B7 III	0.03	125
27 Tau	167 00	-23 15	3.62	B8 III	0.00	125
δ Per	150 17	-05 47	3.01	B5 III	0.04	105
ζ Per	162 17	-16 42	2.85	B1 Ib	0.31	360
ϵ Per	157 21	-10 06	2.89	B0.5 III	0.10	290
π^4 Ori	192 53	-23 32	3.68	B2 III	0.08	450
π^5 Ori	196 15	-24 34	3.73	B2 III	0.05	450
η Ori	204 52	-20 24	3.35	B0.5 Vnn	0.11	450
δ Ori	203 51	-17 45	2.24	O9.5 II	0.08	450
ι Ori	209 32	-19 36	2.77	O9 III	0.07	450
ϵ Ori	205 13	-17 15	1.69	B0 Ia	0.06	450
σ Ori	206 49	-17 20	3.80	O9.5 V	0.06	450
ζ Ori	206 27	-16 36	1.77	O9.5 Ib	0.06	450
κ Ori	214 31	-18 30	2.05	B0.5 Ia	0.04	450
S Mon A	202 56	02 11	4.7	O7	0.08	920
o^2 CMa	235 33	-08 14	3.01	B3 Ia	0.05	860
τ CMa	238 11	-05 33	4.40	O9 Ib	0.13	1050
ρ Leo	234 53	52 46	3.85	B1 Iab	0.05	950
1 Sco	346 06	21 43	4.68	B1.5 Vn	0.19	170
π Sco	347 12	20 14	2.91	B1 V	0.06	170
τ Sco	351 31	12 49	2.81	B0 V	0.05	170
β^1 Sco	353 11	23 37	2.63	B0.5 V	0.20	170
χ Oph	357 56	20 41	4.4	B1.5 Ve	0.53	170
ζ Oph	6 17	23 36	2.56	O9.5 Vnn	0.32	170
α Oph	35 54	22 35	2.07	A5 III	0.00	18
102 Her	47 25	18 26	4.35	B2 IV	0.09	300
δ Cyg	78 42	10 15	2.87	B9.5 III	0.01	50
P Cyg	75 49	01 19	4.8	B1Pe	0.63	1500
α Cyg	84 17	02 00	1.25	A2 Ia	0.09	500
λ Cyg	78 05	-04 20	4.54	B6 IV	0.03	155
59 Cyg	88 02	00 58	4.7	B1.5 Ven	0.21	270
υ Cyg	80 59	-10 03	4.42	B2 Ve	0.14	200
π Aqr	65 59	-44 44	4.64	B1 Ve	0.22	330
o And	102 12	-16 06	3.6	B6 IIIp	0.05	120
2 And	102 30	-15 46	5.04	A2	0.00	19

2.2. *The Instrumental Setup*

The spectra were obtained with the coudé spectrograph of the 2.7 m telescope at McDonald Observatory during five observing runs from 1987 to 1989. All observations were recorded at the D_1 line, rather than the D_2 line, in order to minimize both the saturation of the interstellar lines and interference from the telluric absorption lines also present. The echelle grating was used in the double-pass configuration, with the 800 × 800 TI2 CCD detector placed at the "scanner" focus and with grating C used for cross dispersion. This arrangement allows both high spectral resolution and effective suppression of scattered light to be achieved (Tull 1972). The resulting reciprocal dispersion at the D_1 line is 0.10 Å mm^{-1}, or 0.15 km s^{-1} per 2 pixels of the detector, each pixel being 15 μm wide. A 90 μm entrance slit, corresponding to only 0.″21 on the sky, was used for nearly all of the observations reported here. This slit width yielded an actual instrumental resolution (FWHM) of $\Delta v = 0.5 \pm 0.05$ km s^{-1}, or a resolving power $R = 6 \times 10^5$, deduced from the measured profiles of various comparison lamp lines, as discussed below. The 2 pixel binning of the CCD along the dispersion thus yielded a data format

oversampled by approximately a factor of 3/2. Because of the narrow slit employed (and the unavailability of an image slicer), the various exposure times were strongly governed by the seeing. As a rough benchmark, we note that a signal-to-noise ratio (S/N) = 120 was achieved for ϵ Ori ($V \sim 1.7$) in about 30 minutes in 2″ seeing.

2.3. *Data Reduction*

The initial processing of the CCD frames employed various IRAF routines to subtract the bias, divide by a normalized flat field, and remove cosmic rays from the rows occupied by the stellar spectrum. The one-dimensional spectra were then extracted using the IRAF apextract routines, usually with variance weighting. At each wavelength point, the background at the spectrum was estimated via a low-order polynomial fit to the regions on either side of the spectrum. A smoothed version of this derived background spectrum was subtracted from the stellar spectrum, in order to minimize the contribution of the background spectrum to the noise in the background-subtracted stellar spectrum. The accuracy of the background subtraction was checked via observations of eight stars whose interstellar D lines are expected to be quite saturated (e.g., because the much weaker Na I λ3302 doublet has been detected). The corrections required for (and applied to) those spectra ranged from 0% to 2%. No such correction was applied to the other 30 spectra, whose background levels may thus be uncertain by $\lesssim$2%.

The wavelength calibration was established via observations of a Na/Ne hollow cathode lamp and of an I_2 absorption cell illuminated by the tungsten filament lamp used for the flat-field exposures. Figure 1 shows both a composite I_2 spectrum, constructed from spectra obtained at two different grating settings, and a single Na/Ne spectrum; the velocity zero point is set at the rest wavelength of the stronger Na I hyperfine component (5895.9321 Å). The numerous I_2 absorption lines from the (B–X) system near the Na I D lines have been cataloged and analyzed by Gerstenkorn & Luc (1978, 1979, 1985). The wavenumbers predicted from their derived set of Dunham coefficients generally agree with those measured to within about 0.001 cm^{-1}, or about 0.4 mÅ or 0.02 km s^{-1} at the D lines (Sansonetti 1987). We used the measured wavenumbers (Gerstenkorn & Luc 1978), adjusted for a zero-point offset of -0.0056 cm^{-1} (Gerstenkorn & Luc 1979). At any given grating setting, typically five to six well-spaced, unblended I_2 lines fell within the 50–60 km s^{-1} range observed (Fig. 1); a linear fit to those lines typically yielded rms errors of about 0.3 mÅ. For each grating setting, the wavelength zero points derived from the I_2 and Na/Ne spectra generally agreed to within one data point (0.15 km s^{-1}); the zero point typically varied by less than about one data point (and at most by three data points) over the course of any given night. The dispersion, determined from the fits to the I_2 spectra, varied by less than about 0.1% (i.e., less than about 0.06 km s^{-1} over the whole spectrum) during an individual night, and by less than about 0.2% from night to night; an average dispersion was adopted for several nights for which we had no I_2 spectra. Many stars were observed more than once during the course of this survey; the zero-point differences among such multiple spectra were always less than 0.5 km s^{-1}, and were usually less than about 0.2 km s^{-1}, with no apparent systematic night to night offsets. Those differences include the uncertainties due to the fitting of the interstellar line profiles; the velocities in any individual spectrum are apparently typically accurate to 0.2–0.3 km s^{-1}.

The individual wavelength-calibrated spectra were then normalized via fits of Legendre polynomials (generally of order 11–15) to sections free of interstellar or telluric absorption. Some of those individual spectra exhibited low-level undulations which could have been due to weak, broad interstellar absorption; those possible weak "features" were generally not consistent among multiple spectra for the same star, however, and generally did not correspond to components known from lower resolution observations of Na I or Ca II. Since multiple spectra otherwise showed quite good mutual agreement, those low-level undulations (which occasionally occurred even in spectra of telluric standard stars) were considered to be spurious, and were normalized out. It is possible, however, that some genuinely interstellar broad, very weak absorption components may have been normalized out in a few cases. Because the interstellar absorption toward 12 of the 38 stars spans

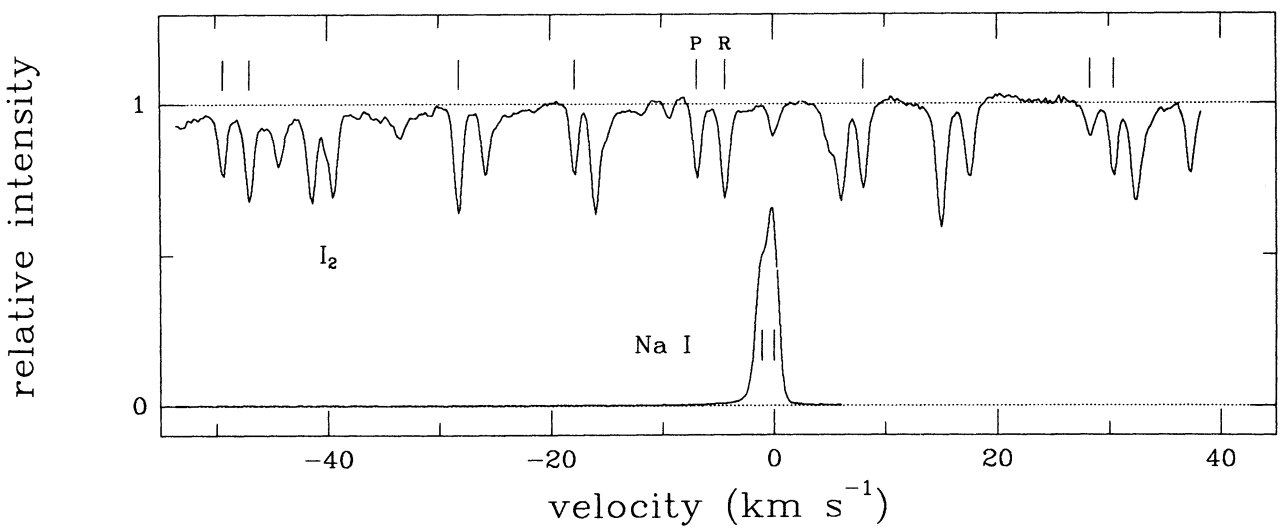

FIG. 1.—At the top is a composite I_2 absorption spectrum, constructed from spectra obtained at two different grating settings. The narrow (observed FWHM $\sim$ 0.85 km s^{-1}), unblended lines used in the wavelength calibration are noted with tick marks. The lines marked P and R are the P(54) and R(59) lines of the 15–2 band, which were used in determining the instrumental resolution. Below is a single Na/Ne emission spectrum, showing the partially resolved hyperfine structure in the Na I D_1 line. The velocity zero point is set by the wavelength of the stronger D_1 hyperfine component (5895.9321 Å). Note also the slight blueward tail on the Na I emission line, which may be due to a slight amount of charge transfer inefficiency in the TI CCD used for the observations.

about half, or occasionally more, of the 50–60 km s^{-1} range recorded in a single exposure, some uncertainty exists in each of those cases in correctly interpolating the continuum across the regions of interstellar absorption. In most cases, though, that uncertainty should amount to no more than several percent. The uncertainty may be larger, however, for the relatively sharp-lined A2 Ia star α Cyg, whose unnormalized spectra exhibit strong stellar D_1 absorption. Stellar lines are not troublesome for the other stars in our sample, as they are of earlier spectral types and generally have significantly larger projected rotational velocities.

The individual normalized spectra were then brought to a common heliocentric velocity scale with a grid spacing of 0.1 km s^{-1}, with slight additional shifts made in the 21 (of 38) cases where we had multiple spectra in order to more precisely align the interstellar absorption lines. Where we had multiple spectra, the individual spectra were weighted by the inverse of the rms deviation of the continuum fit, then summed. The summed spectra were then resampled by adding adjacent pixels onto a wavelength grid with spacing 0.004 Å, or 0.2 km s^{-1}. The S/N and the total equivalent width of the interstellar D_1 line which were measured from these final, summed spectra are listed for each star in columns (2) and (3) or columns (9) and (10) of Table 2. With one exception (ϵ Ari A), the empirical S/N, derived from rms fluctuations in the continuum, ranged from about 45 to 280, with an average value of 105. That average S/N yields a 2 σ equivalent width limit or uncertainty for narrow lines of about 0.5 mÅ (photon noise plus continuum placement uncertainty), which corresponds to a Na I column density of 5×10^9 cm^{-2}.

When the spectral interval to be observed included absorption features due to telluric H_2O (see, e.g., Hobbs 1978a), stars with no detectable interstellar Na I absorption were observed as telluric standards in order to gauge the location and significance of any telluric absorption. There were no cases of serious overlap between interstellar Na I and telluric H_2O absorption, so features due to the latter have been fitted by Gaussians and removed from the final spectra. Our spectra are of sufficient resolution and S/N to also detect and resolve absorption from telluric Na I, which is of some current interest due to the use of the Na I layer for creating laser guide stars in some adaptive optics schemes. The telluric Na I absorption is apparent in some spectra obtained during the fall (see γ Cas, κ Ori, and α Oph in Fig. 2; also in spectra of several telluric standard stars not shown), but is absent in those obtained during the summer. Profile fits indicate a maximum column density per unit air mass (during November) of about 7×10^9 cm^{-2} and a b-value of 0.36 ± 0.05 km s^{-1}, which corresponds to a maximum temperature of about 175 K. Within the uncertainties in the data and in our adopted instrumental FWHM, these values are in good agreement with the $N(\mathrm{Nov}) = (6 \pm 2) \times 10^9$ cm^{-2}, seasonal variations in N, and $T = 200$ K derived from lidar observations of the Na I layer (e.g., Megie et al. 1978; Jeys 1991; see also McNutt & Mack 1963). The geocentric velocities of the telluric Na I lines are all within about 0.3 km s^{-1} of zero, providing additional confirmation of the accuracy of the velocity zero points. Only in the case of the weak Na I absorption toward α Oph does the telluric Na I line interfere significantly with the interstellar Na I absorption (see § 5.1 below).

2.4. *Instrumental Resolution*

In Paper I, we estimated our achieved resolution as 0.6 ± 0.1 km s^{-1}, based primarily on preliminary analyses of the I_2 and Na I calibration spectra. Information obtained since then on the intrinsic widths of thorium lines in Th/Ar hollow cathode lamp spectra, and comparisons of some of the Na I spectra reported here with spectra recently obtained with the Ultra High Resolution Facility (UHRF; ~ 0.3 km s^{-1} resolution) at the Anglo-Australian Observatory, however, have led to a more precise estimate for the resolution characterizing the present data: 0.5 ± 0.05 km s^{-1}, as noted above. This estimated resolution yields consistency among a number of different indicators.

Each of the I_2 rotational lines actually consists of a number of hyperfine-split subcomponents; differences in the relative intensities of the various groups of subcomponents lead to systematic differences in the widths of the lines for even and odd J'' (0.0237 cm^{-1} and 0.0267 cm^{-1}, respectively; Kroll & Innes 1970). The $P(54)$ and $R(59)$ lines of the 15–2 band lie quite close to the rest wavelength of the D_1 line (Fig. 1), and were observed in all our I_2 exposures, with average FWHM of 0.82 ± 0.05 and 0.87 ± 0.05 km s^{-1}, respectively. If we assume that the measured line widths are due to a combination of the intrinsic hyperfine structure (0.42 and 0.47 km s^{-1}), thermal broadening at $T \sim 300$ K (0.23 km s^{-1}), and instrumental broadening, we derive an instrumental FWHM of 0.51 ± 0.08 km s^{-1}. The above intrinsic widths due to hyperfine structure are strictly applicable to weak absorption lines ($\tau \lesssim 0.2$); the instrumental FWHM derived from these somewhat stronger I_2 lines may thus be a slight overestimate.

Observations of Th/Ar hollow cathode lamp spectra at resolutions sufficient to resolve the thorium lines have recently been obtained using the Kitt Peak National Observatory Solar FTS (0.24 km s^{-1} resolution; Willmarth 1994) and using the Anglo-Australian Observatory's UHRF (0.32 km s^{-1}; Welty, Morton, & Hobbs 1994b; see also Crawford et al. 1994). The derived intrinsic (thermally broadened) thorium line widths (FWHM) were 0.56 ± 0.01 km s^{-1} and 0.54 ± 0.01 km s^{-1}, respectively. With a slight adjustment to our setup at Na I D_1, we observed the Th I line at 5760 Å to have a FWHM of 0.76 km s^{-1}. If we assume an intrinsic width of 0.55 ± 0.02 km s^{-1} for the line (essentially assuming our Th/Ne lamp to have a similar operating temperature to the Th/Ar lamps measured at higher resolution), then that observed FWHM implies an instrumental FWHM of 0.52 ± 0.02 km s^{-1}.

Comparisons of the b-values derived from narrow lines in the present Na I spectra with those derived from other Na I spectra obtained at comparable or higher resolution (δ Cyg and α Cyg: Blades et al. 1980; ζ Oph: Barlow et al. 1994; ϵ Ori: Welty et al. 1994b) seem to imply an achieved resolution for these data of about 0.5 km s^{-1}, or perhaps slightly better. The observed widths of the telluric Na I lines and of the λ6328 line from a He/Ne laser also suggest that the instrumental resolution could be slightly better than 0.5 km s^{-1}. In view of these various observations and comparisons, we adopt 0.5 ± 0.05 km s^{-1} as the best estimate for our achieved resolution.

3. RESULTS

3.1. *The Spectra*

The observed line profiles are shown in Figure 2, where plus signs represent the observed data and the solid lines give the adopted multicomponent fit, as described below. The velocity scale is with respect to the stronger of the two Na I D_1 hyperfine components (rest wavelength 5895.9321 Å; see Appendix

A); the tick marks above the profiles mark that stronger hyperfine component for each interstellar cloud determined in the fit. At least 29 examples of resolved hfs components are immediately apparent in the spectra; these cases are indicated by a superscript "a" in column (4) or column (11) of Table 2. Each such line pair is indeed split by about 1.08 km s^{-1}, and the component at the longer wavelength is stronger by approximately the factor 5/3 which obtains in the optically thin limit. A comparable number of components are similarly narrow, but are blended with other components within about 1.5 km s^{-1}. Many of the profiles show subtle but definite asymmetries and inflections that indicate the presence of multiple, closely spaced, blended components; such structure has not been discernible in the generally lower resolution and/or lower S/N

TABLE 2

COMPONENT PARAMETERS

Star	S/N	W_λ (mÅ)	Comp	$v_\odot$ (km s^{-1})	N_{10} (10^{10} cm^{-2})	b (km s^{-1})	Star	S/N	W_λ (mÅ)	Comp	$v_\odot$ (km s^{-1})	N_{10} (10^{10} cm^{-2})	b (km s^{-1})
γ Cas	150	49.1	1	-7.30	25.5	2.47	η Ori	75	164.6	1	3.85	1.9	(0.50)
			2[a]	-5.06	17.1	0.61				2	5.06	12.9	[0.45]
			3	-3.72	3.4	0.37				3	[6.20]	[230.0]	[0.50]
			4[a]	-2.79	10.3	0.41				4	[8.30]	[300.0]	[1.15]
			5	-1.25	2.1	1.57				5	10.07	10.9	[0.60]
										6	[11.00]	10.8	[0.80]
ϵ Ari A	20	120.	1	11.50	72.8	1.39				7	12.90	5.3	[0.60]
			2	15.72	164.0	1.51				8	15.17	3.2	[0.50]
										9	16.37	4.1	(0.80)
17 Tau	100	18.4	1	15.80	17.1	1.13				10	24.82	21.7	[0.55]
			2	18.22	3.0	0.59				11	25.38	14.7	[0.80]
										12	27.96	2.6	[0.80]
η Tau	85	41.7	1	16.33	63.2	1.10							
							δ Ori	120	42.6	1	5.55	1.6	1.64
27 Tau	80	68.9	1	14.36	4.7	[1.00]				2	9.33	6.0	1.89
			2	16.19	148.0	0.76				3	15.17	2.6	0.88
			3	17.37	20.1	0.64				4	21.81	10.0	1.26
			4	18.58	4.8	[1.00]				5	24.48	14.0	[1.05]
										6[a]	25.24	8.9	0.49
δ Per	135	9.9	1	4.71	3.3	1.28				7	26.55	5.0	0.40
			2	5.93	7.3	0.68							
							ι Ori	140	43.6	1	-1.60	1.5	1.90
ζ Per	50	150.8	1	9.80	4.7	[0.85]				2	1.63	2.4	1.81
			2	11.12	52.6	[0.90]				3	8.41	18.5	0.64
			3	[12.24]	[300.0]	(1.00)				4	11.88	0.6	0.92
			4	[13.74]	[3750.0]	[0.75]				5	18.01	0.7	0.98
			5	[14.90]	[4000.0]	[0.75]				6	[20.70]	0.7	(1.50)
			6	[16.35]	69.2	[0.40]				7	23.55	2.7	[0.40]
			7	17.27	3.0	[0.40]				8	25.07	10.6	1.09
										9	26.55	1.2	[0.40]
ϵ Per	90	89.6	1	4.82	6.7	0.72				10	31.90	1.6	1.60
			2	7.03	83.0	0.90				11	33.72	7.9	[0.95]
			3	8.60	28.2	(0.80)							
			4	9.97	36.6	0.70	ϵ Ori	155	139.6	1[a]	2.99	7.7	0.36
			5	12.72	1.5	1.25				2	4.98	5.4	1.48
			6	20.01	1.8	2.28				3	8.59	5.2	(1.45)
										4	11.03	34.1	0.74
π^4 Ori	85	63.1	1	21.01	3.2	0.52				5	12.47	14.4	0.51
			2	23.77	73.9	1.01				6[a]	14.77	6.5	0.53
			3	25.09	15.7	0.57				7[a]	17.28	18.4	0.49
			4	26.41	6.2	0.85				8	18.50	1.4	(1.00)
			5	28.61	3.1	0.71				9	22.75	12.8	0.52
										10	23.95	13.2	0.57
π^5 Ori	55	95.7	1	12.57	6.7	1.35				11[a]	24.88	52.9	0.51
			2	17.33	6.0	1.75				12	26.04	21.5	0.88
			3	21.15	27.7	0.67				13	28.13	7.2	0.73
			4	23.14	147.0	0.67							
			5	24.32	30.0	[0.80]	σ Ori	85	145.0	1	0.00	5.8	1.93
			6	26.74	4.8	1.24				2	6.31	12.7	3.94
										3	12.11	0.9	0.47
										4	19.16	3.6	[1.15]
										5	19.95	105.0	[0.65]
										6	21.11	39.6	[1.15]
										7	24.17	107.0	0.54
										8	25.18	21.5	0.47
										9	26.08	19.1	[0.95]

spectra previously available. A few selected profiles are shown at an expanded velocity scale in Figure 3 to illustrate some of the subtle structure revealed at the relatively high resolution and S/N of these new spectra (see also Fig. 2 of Paper I).

3.2. *Profile Analysis*

We have used the method of profile fitting in an attempt to discern and determine the properties of the individual interstellar clouds contributing to the observed absorption-line profiles (Welty, Hobbs, & York 1991, and references therein). We assumed each distinct cloud to be characterized by a column density N (with the Na I hyperfine levels populated according to their statistical weights [5/3]), by a bulk cloud velocity v, and by a Maxwellian internal velocity distribution described by the line width parameter b (see also Appendices A and B). We used the minimum number of components needed

TABLE 2—*Continued*

Star	S/N	W_λ (mÅ)	Comp	$v_\odot$ (km s^{-1})	N_{10} (10^{10} cm^{-2})	b (km s^{-1})	Star	S/N	W_λ (mÅ)	Comp	$v_\odot$ (km s^{-1})	N_{10} (10^{10} cm^{-2})	b (km s^{-1})
ζ Ori	135	137.1	1	-5.69	5.2	1.12	1 Sco	75	179.8	1	-19.14	4.3	(1.00)
			2	-1.74	27.6	2.31				2	-16.87	89.8	0.90
			3	10.09	8.0	2.60				3	-13.89	42.6	1.02
			4	11.73	2.9	0.45				4	-12.17	10.8	[0.60]
			5	13.12	2.0	1.04				5	-8.63	251.0	0.81
			6	18.77	7.3	0.99				6	-6.70	64.8	0.68
			7	[21.70]	1.9	(0.75)				7	-5.11	3.1	(1.00)
			8	23.18	64.5	[0.54]							
			9	23.81	26.4	[0.70]	π Sco	120	40.7	1	-22.18	2.9	1.04
			10	26.39	60.1	[0.90]				2	-16.89	13.6	(1.50)
			11[a]	26.45	18.5	[0.35]				3[a]	-15.90	14.6	0.50
										4	-14.94	6.0	[0.40]
κ Ori	110	117.5	1	0.40	17.0	4.25				5	-14.18	3.8	0.63
			2	4.13	9.2	2.30				6[a]	-12.56	4.8	0.50
			3	17.64	11.1	(1.00)				7	-7.11	2.6	0.90
			4	18.19	18.0	0.38							
			5	19.11	25.6	[0.40]	τ Sco	135	41.4	1	[-9.90]	1.9	[0.50]
			6	20.67	101.0	[0.75]				2[a]	-8.84	38.0	0.41
			7	21.63	21.5	[0.55]				3	-7.89	6.2	[0.50]
			8	23.60	11.2	1.03				4	-6.32	4.1	(0.80)
										5[a]	-4.45	8.6	0.57
S Mon A	55	88.1[b]	1[a]	-2.11	4.6	0.51							
			2	5.07	5.7	0.83	β^1 Sco	125	140.4	1	-23.36	7.0	[0.52]
			3	7.15	6.3	[1.20]				2	-22.04	6.8	(2.00)
			4	10.48	9.6	[1.50]				3	-15.14	4.8	(1.50)
			5	12.22	6.6	0.58				4	-12.81	28.8	[0.54]
			6	14.33	2.4	0.35				5	-10.18	[700.0]	(1.00)
			7	18.69	7.5	[0.70]				6	-8.34	83.5	[0.80]
			8	21.10	17.4	[1.50]				7	-6.82	9.1	[0.75]
			9[a]	23.79	14.1	0.32							
			10	24.78	27.1	0.61	χ Oph	90	203.8	1	-27.59	1.5	(0.90)
			11	26.06	5.6	[0.90]				2	-23.98	3.3	(0.70)
										3	-21.61	13.2	(0.80)
o^2 CMa	65	28.9	1	15.95	10.0	3.74				4	-20.58	13.3	[0.45]
			2	19.49	4.4	1.03				5	-19.84	9.1	[0.33]
			3	26.85	15.7	6.15				6	-18.61	8.4	[1.00]
										7	-16.12	7.7	[1.00]
τ CMa	45	195.2	1	11.97	2.2	0.77				8	-13.05	150.0	[0.85]
			2	15.70	14.4	2.99				9	[-11.40]	[13000.0]	[0.70]
			3	19.40	9.8	0.82				10	[-9.80]	[600.0]	[0.70]
			4	21.97	6.8	[1.00]				11	-8.60	118.0	[0.90]
			5	25.09	51.5	1.12				12	-7.00	9.2	(0.80)
			6	28.38	11.1	0.71				13[a]	-4.69	2.7	[0.33]
			7	30.86	54.5	[0.80]							
			8	32.60	51.7	[0.85]	ζ Oph	200	188.1	1	-28.70	8.5	[1.20]
			9	34.30	43.8	[2.50]				2[a]	-28.32	2.1	[0.25]
			10	38.92	10.4	(2.00)				3	-26.51	0.9	[0.45]
			11	43.08	20.5	1.12				4[a]	-25.89	1.9	[0.35]
			12	45.44	1.7	(1.00)				5	-20.64	7.3	(0.80)
										6	-19.08	69.7	0.76
ρ Leo	70	85.2	1	-12.82	7.3	(1.20)				7	-16.44	125.0	[0.65]
			2	-11.16	16.3	[0.60]				8	[-14.95]	[5500.0]	[0.60]
			3	-8.70	18.7	[1.10]				9	[-13.95]	[3500.0]	[0.49]
			4	-7.12	4.8	(0.80)				10	-12.65	68.9	0.67
			5	-4.99	13.0	1.09				11	-11.13	7.7	(0.80)
			6[a]	-1.24	12.2	0.44				12[a]	-9.04	5.8	0.40
			7	18.26	30.7	0.58							

TABLE 2—*Continued*

Star	S/N	W_λ (mÅ)	Comp	$v_\odot$ (km s^{-1})	N_{10} (10^{10} cm^{-2})	b (km s^{-1})	Star	S/N	W_λ (mÅ)	Comp	$v_\odot$ (km s^{-1})	N_{10} (10^{10} cm^{-2})	b (km s^{-1})
α Oph	280	2.8	1	-26.15	2.5	[2.15]	λ Cyg	85	122.2	1	-21.26	4.4	0.65
			2	-22.44	0.3	(1.50)				2	-19.42	4.6	(0.80)
										3	-16.39	19.8	[0.65]
102 Her	95	68.0	1	-26.54	2.8	(3.00)				4	-15.35	5.7	[0.60]
			2	-21.86	12.9	(3.00)				5	-12.24	13.5	[0.65]
			3[a]	-19.55	15.2	0.40				6	-10.21	93.7	0.99
			4	-18.34	26.4	[0.80]				7	-6.91	3.3	0.63
			5	-17.00	11.8	0.81				8[a]	-5.28	25.1	0.49
			6	-15.39	16.7	0.61				9	-3.73	15.2	0.55
			7	-14.09	0.8	[0.60]							
			8	-4.19	1.3	0.95	59 Cyg	70	141.8	1	-25.32	1.8	[0.50]
										2	-22.11	118.0	0.80
δ Cyg	130	20.2	1[a]	-18.54	29.6	0.42				3	-20.14	29.9	0.50
										4	-11.76	24.7	[0.57]
P Cyg	90	389.1[b]	1	-24.38	3.8	[0.60]				5	-10.33	22.6	0.76
			2	-22.24	11.8	(1.00)				6	-9.63	70.9	[0.45]
			3	-19.64	[225.0]	[0.90]				7	-8.94	29.7	[0.50]
			4	-17.11	[387.0]	[0.85]				8	-7.60	2.8	(1.00)
			5	-14.69	[189.0]	[1.00]							
			6	-12.74	[172.0]	[0.80]	υ Cyg	120	77.5	1[a]	-24.20	8.5	0.54
			7	-11.04	[180.0]	[0.50]				2[a]	-21.59	9.3	[0.55]
			8	-9.90	[300.0]	[0.50]				3	-19.97	5.7	[0.65]
			9	-8.50	[378.0]	[1.10]				4	-16.91	14.3	1.11
			10	-6.10	[88.3]	[1.20]				5	-14.20	3.8	[0.65]
			11	-4.40	29.8	[0.70]				6	-12.90	62.7	0.86
			12	-3.16	9.9	[0.90]				7	-9.71	1.8	(1.00)
			13	-0.91	10.5	[0.90]							
			14[a]	0.10	20.8	0.43	π Aqr	55	220.8	1[a]	-17.12	16.6	0.38
			15	1.14	5.9	(0.80)				2	-13.66	79.5	[1.60]
			16	2.29	4.9	[0.70]				3	-12.11	26.7	(0.80)
										4	-11.01	53.5	0.87
α Cyg	180	240.4	1	-21.79	156.0	0.58				5	-7.53	33.4	[0.50]
			2	-20.78	22.2	0.39				6	-5.63	195.0	[1.00]
			3	-13.22	123.0	0.54				7	-1.75	36.5	0.87
			4	-11.99	47.4	[0.70]				8	-0.23	18.0	0.58
			5	-9.54	38.5	0.47							
			6[a]	-8.22	67.7	0.58	o And	120	189.2	1	-20.55	55.2	0.51
			7	-6.00	27.6	1.62				2	-19.77	84.0	[0.75]
			8	-3.85	10.8	0.46				3	-18.16	2.1	(0.80)
			9[a]	-2.78	30.3	0.40				4	-13.46	3.2	[1.15]
			10[a]	1.33	29.6	0.38				5	-10.63	48.4	1.02
			11	5.53	0.9	0.44				6	-8.47	192.0	0.80
										7	-6.41	119.0	0.93
										8	-4.01	4.4	(0.60)
										9	-3.54	2.7	[0.35]
							2 And	55	35.0	1	-10.02	10.9	0.57
										2	-7.98	34.3	0.93

NOTE.—Parameters enclosed in parentheses and brackets were fixed in the profile fitting. Those in brackets are about as well determined as the parameters which were allowed to vary; those in parentheses are less well determined.

[a] Component displays immediately recognizable hyperfine structure.

[b] Additional Na I absorption is present outside the velocity range observed in this study.

to adequately fit each profile—i.e., such that the rms deviation between the data and the fitted profile was comparable to the previously determined continuum rms and such that there were no "obvious" additional components needed. In general, all three parameters (N, b, v) for each component were allowed to vary in the iterative nonlinear least-squares fit to the observed profile; some parameters were occasionally held fixed at "reasonable" values in order to facilitate convergence of the fit, however. In a few cases of very strong lines (ζ Per, η Ori, β^1 Sco, χ Oph, ζ Oph, P Cyg), parameters were constrained via information from the weaker Na I λ3302 doublet (Crutcher 1975; Hobbs 1978b; Meyer & Roth 1991; Crawford 1992), the λ7698 line of K I (Hobbs 1974a; Welty et al. 1994b), or other transitions observed at high resolution and S/N (e.g., the CN λ3874 line toward ζ Oph observed by Lambert, Sheffer, & Crane 1990). The scaling of Na I column density from K I column density is somewhat arbitrary (though reasonable) for a few of the most blended components in several of those lines of sight. Table 2 presents the parameters for the adopted line profile fits. Successive columns give the star name, continuum

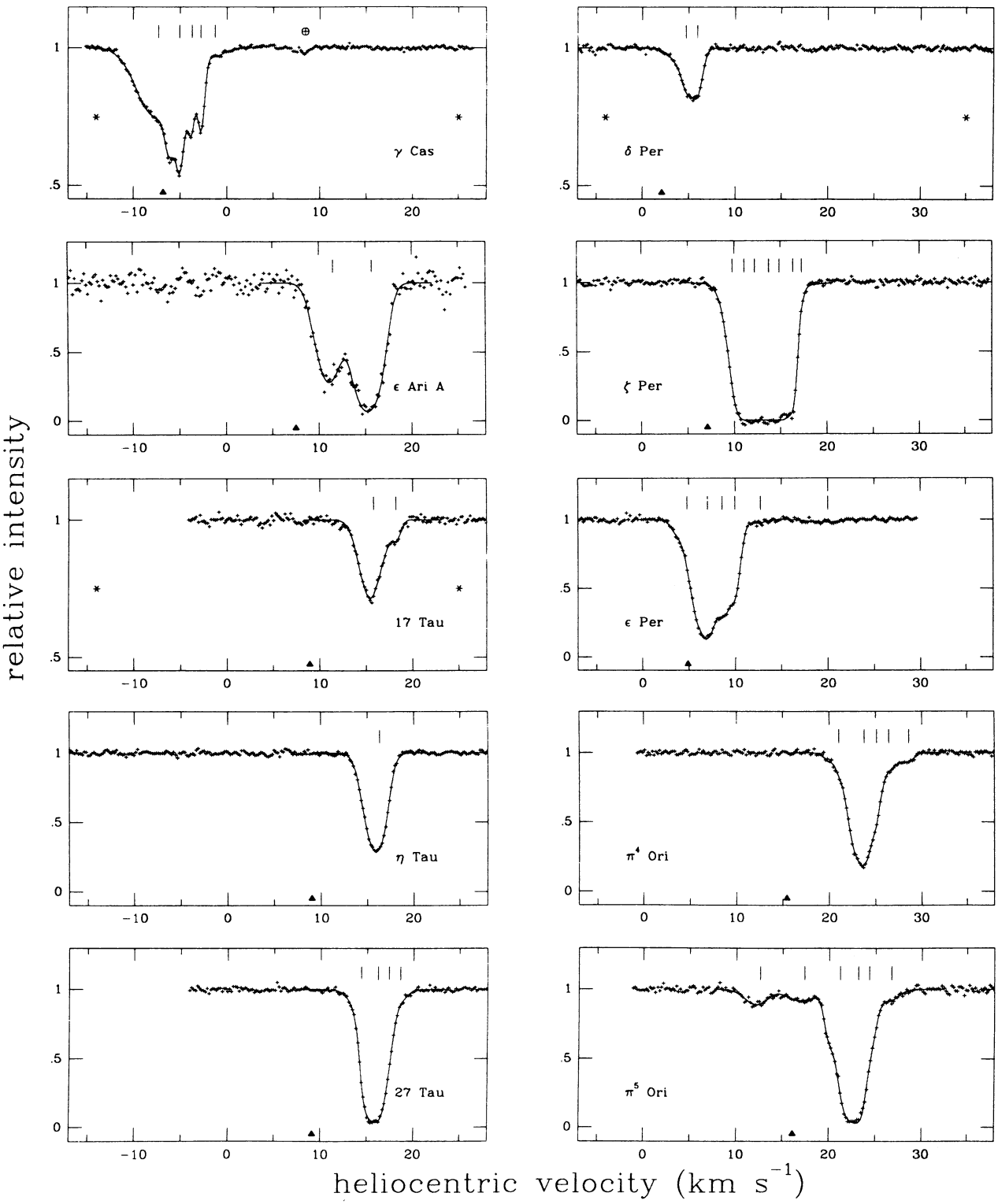

FIG. 2*a*

FIG. 2.—The observed interstellar Na I D_1 absorption-line profiles are given by the crosses, with the individual data points separated by 0.2 km s^{-1}. Stellar lines have been removed from these normalized profiles. The solid line shows the adopted fitted profile, as described in the text (§ 3.2). The velocities are heliocentric and are referred to the stronger of the two hyperfine split subcomponents of the D_1 line. The tick marks give the location of that stronger subcomponent for each interstellar cloud adopted in the fitted profile; the corresponding weaker subcomponent is located 1.08 km s^{-1} to the blue. Narrow hyperfine split components are visible in many cases; see δ Cyg for a particularly clear example. The zero point for LSR velocities is shown by the solid triangle. Weak telluric Na I absorption (crossed circle) is noted toward γ Cas, κ Ori, and α Oph. The second o And spectrum shows the extra absorption present during a shell phase. The vertical scale has been expanded in a few cases to show weaker lines more clearly (noted by an asterisk near the vertical axes).

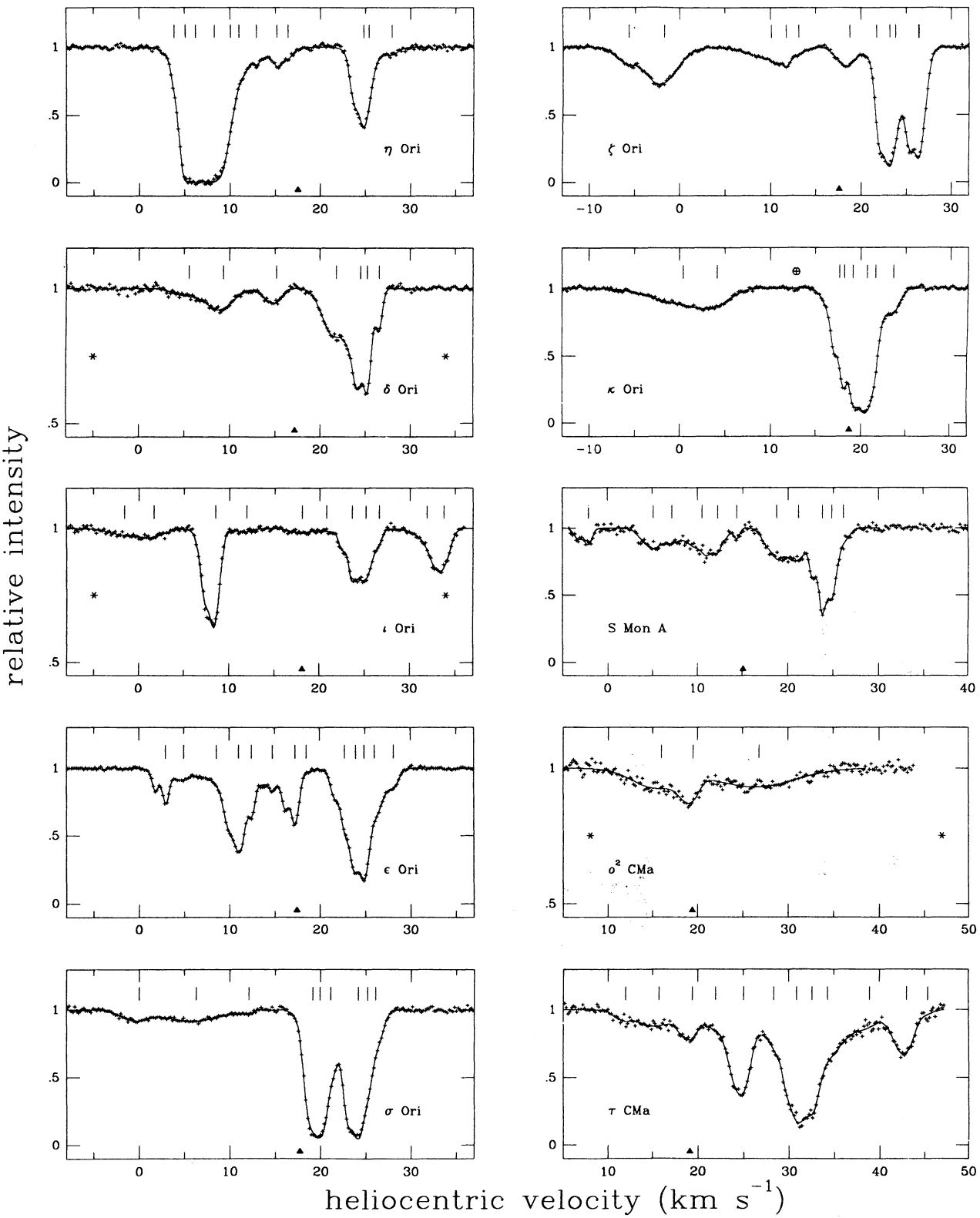

FIG. 2*b*

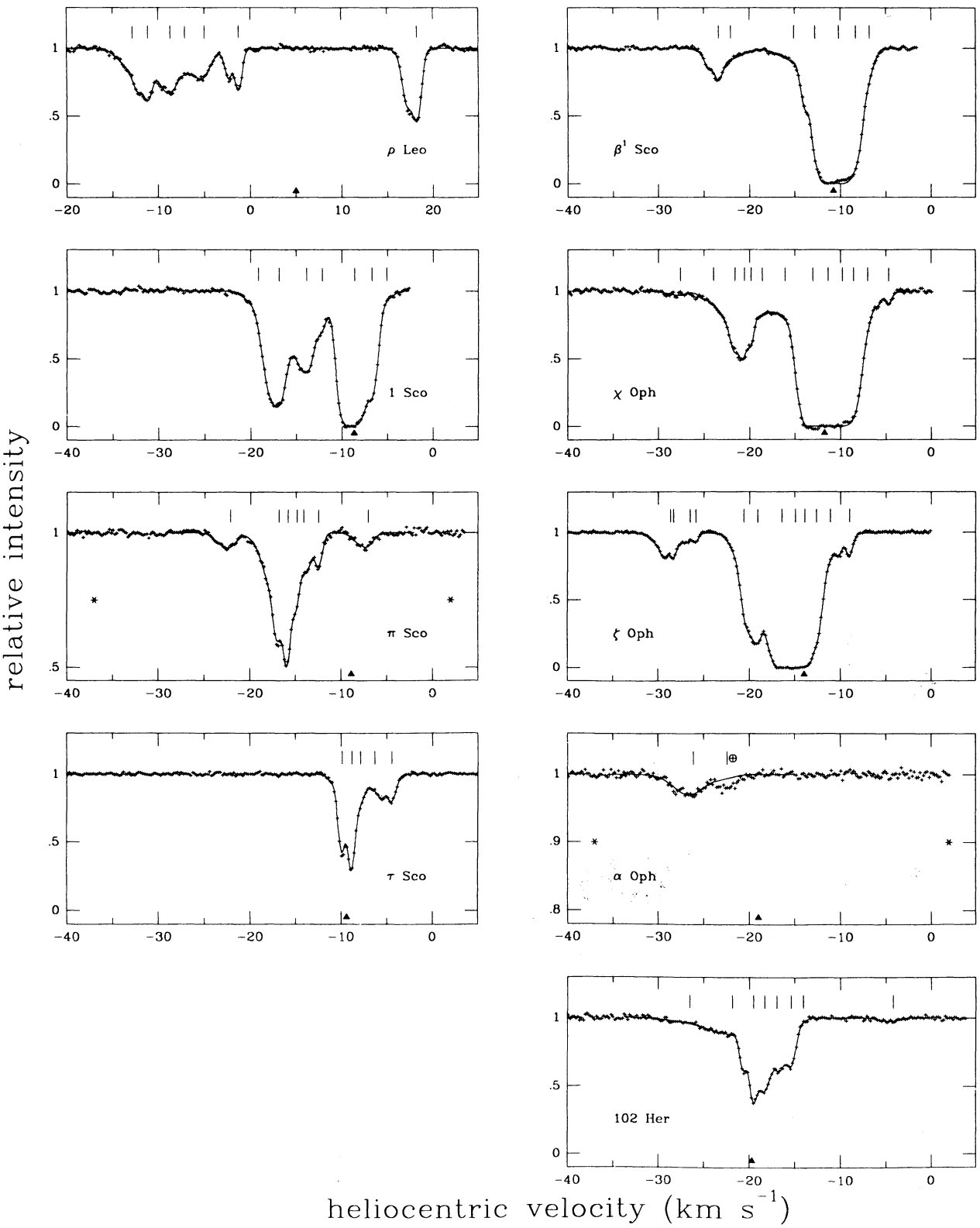

FIG. 2c

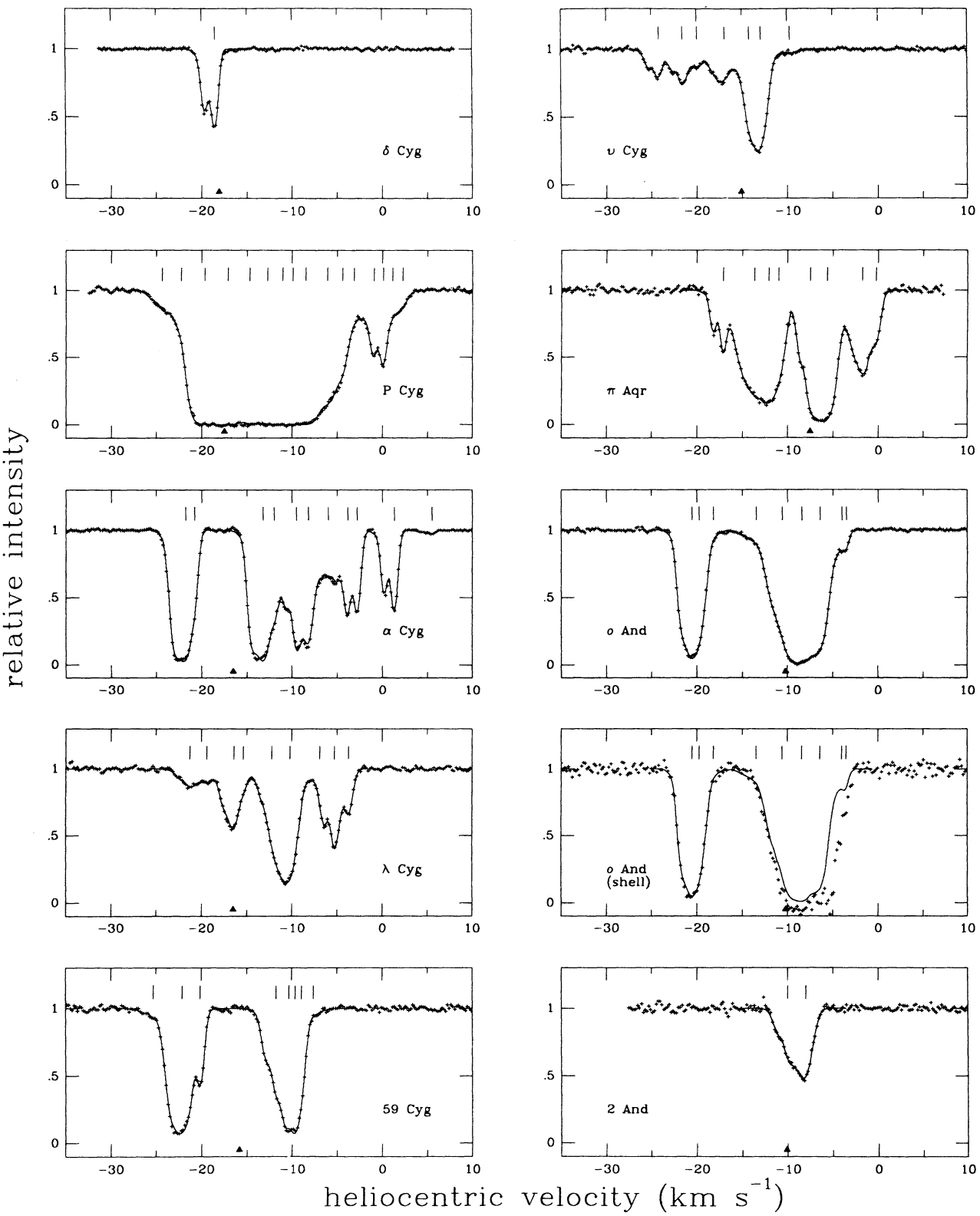

FIG. 2*d*

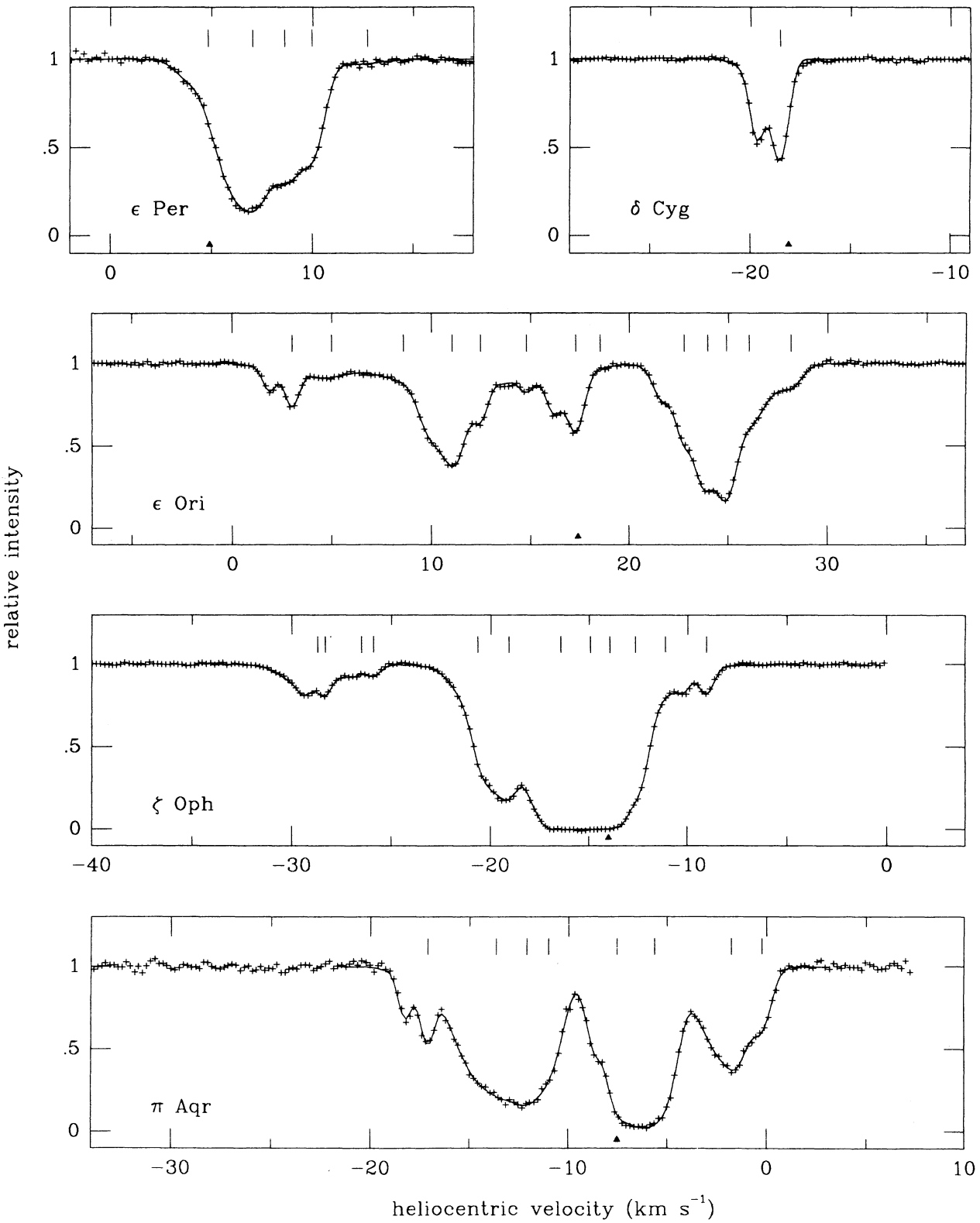

FIG. 3.—The Na I profiles for ϵ Per, δ Cyg, ϵ Ori, ζ Oph, and π Aqr are shown at an expanded velocity scale, to illustrate the subtle asymmetries and inflections—indicating the presence of multiple narrow, closely blended components—which may be discerned in these new high-resolution spectra. Such fine profile structure has not been discernible in previous spectra obtained even at resolutions ~ 1 km s^{-1}.

S/N, total equivalent width, component number, heliocentric velocity, column density, and b-value. The parameters held fixed in the fitting are enclosed either in parentheses or in square braces. Those in braces are thought to be determined about as well as those parameters which were allowed to vary, while those in parentheses are somewhat less well determined.

Our initial fits assumed a Gaussian instrumental function. We found, however, that the two hyperfine subcomponents due to apparently single, cold, isolated clouds (e.g., toward δ Cyg) were not fitted well in detail, and that the cores of some strong lines seemed to be asymmetric in the wrong sense (i.e., weaker absorption toward the red), inconsistent with the reasonable assumption of a 5/3 population ratio for the two hfs levels. In addition, the Na I lamp lines showed a slight blueward tail (Fig. 1), suggestive of a slight asymmetric tail in the instrumental function. These effects may plausibly be attributed to a slight amount of charge transfer inefficiency, which is known to afflict other TI CCDs. Addition of a slight asymmetric tail to our instrumental function noticeably improved the fits to isolated narrow hyperfine pairs and to the cores of some of the strong lines. We note, however, that the number of components needed to adequately fit a given profile was not changed, and that the derived component parameters were not much changed—the main effect was to slightly lower the b-values (by several hundredths of a km s^{-1} for $b \lesssim 0.6$ km s^{-1}).

Even with the use of a modified instrumental function, many of the stronger absorption features were still not fitted well in the cores, however. Furthermore, for spectra with S/N > 50, no strong feature with total $N \gtrsim 7 \times 10^{11}$ cm^{-2} could be adequately fitted with a single component—either at the edges or in the core. Such strong features are likely to be made up of multiple narrow, closely blended line components that cannot be unambiguously disentangled even at our resolution and S/N. The combined effects of our finite resolution (0.5 km s^{-1}) and the Na I D_1 hyperfine splitting (1.08 km s^{-1}) make it increasingly difficult to resolve components separated by less than about 0.8 km s^{-1}, especially for strong lines. Alternatively, our assumption of a Maxwellian internal velocity distribution for each individual component could be invalid for these strong features. Observations of weaker lines (e.g., Na I λ3302, K I λ7698), at comparably high resolution and S/N, are needed to better defne the component structures in such cases.

Formal uncertainties in the fitted parameters may be estimated via the diagonal terms in the matrix inverted to calculate parameter increments as the fit converges, under the assumptions that (1) the component structure has been accurately determined, (2) the fit has converged, and (3) the rms deviation betwen the data and the fit is representative of the noise present in the data. For relatively narrow, isolated lines of moderate strength, those formal (roughly 1 σ) uncertainties are typically a few times 10^9 cm^{-2} for N (as expected from the equivalent width uncertainties), and a few hundredths of a km s^{-1} for b and v. For stronger, wider, and more blended lines, the uncertainties in N are typically 5%–20%; the uncertainties in b and v are typically 0.1–0.3 km s^{-1}. For the strongest lines, uncertainties in the actual component structure are likely to be dominant. Additional systematic errors, due to errors in the adopted background level, in the continuum fit, and/or in the adopted instrumental FWHM, are also possible, but are likely to be minor in most cases. The 0.05 km s^{-1} uncertainty in the adopted instrumental FWHM, for example, implies an uncertainty in the b-values derived from fitting the line profiles of 0.03 and 0.01 km s^{-1} for b-values of 0.4 and 0.8 km s^{-1}, respectively.

3.3. *Comparisons with Other Work*

In Paper I, we made preliminary comparisons of our new data (for six lines of sight) with two previous high-resolution studies; we now extend those comparisons to our full sample. We have observed all three of the stars (η Tau, δ Cyg, and α Cyg) reported by Blades et al. (1980), who used a Michelson interferometer at a resolution of about 0.5 km s^{-1}. For the isolated, well-determined components in those three lines of sight, the velocities agree to within 0.1 km s^{-1}, our b-values are smaller by several hundredths of a km s^{-1}, and the column densities agree to within about 15%. The agreement is well within the uncertainties of both studies. The details of the component structure derived for the blended features in the spectra of α Cyg are somewhat different in the two studies, however, and we do not require a second, weaker component toward η Tau. These differences are likely due to several factors: the intrinsic difficulty in unambiguously determining component structures for unresolved blends, combined with the differences in instrumental profile, S/N achieved, and (possibly) degree of telluric contamination in the two studies.

Most of the stars in this survey had been observed previously by Hobbs (1969a, 1976, 1978b) with the PEPSIOS interferometric scanner at a resolution of approximately 1 km s^{-1} (estimated by comparison with the present data); lower resolution data often were available as well. With only a few exceptions (notably ι Ori), the total equivalent widths agree within their mutual 2 σ uncertainties. Discrepancies can generally be ascribed to differences in the continuum determination (some of the PEPSIOS spectra have limited spectral coverage and/or poorer S/N), to the presence of telluric lines in some of the PEPSIOS scans, or to limitations in the present spectral coverage. The apparent -0.5 km s^{-1} difference (new minus PEPSIOS) in the velocity zero points between the two studies, noted for the six stars in Paper I, is confirmed for the full sample presented here. For 41 comparisons between high-resolution data (new D_1 vs. old D_1 and/or D_2), the apparent offset is -0.58 ± 0.35 km s^{-1}. No systematic trends have yet been identified (e.g., with brightness, night observed, hour angle); at least part of the offset may be due to differences in illumination of the circular PEPSIOS entrance aperture for the stellar and wavelength calibration scans, however. The velocity scales seem to be consistent, apart from the case of α Cyg noted in Paper I.

Three stars in our sample (γ Cas, δ Per, η Tau) have also been observed by Welsh, Vedder, & Vallerga (1990) and Welsh et al. (1991) at a resolution of about 2 km s^{-1} and fairly high S/N. For each of those three stars, the velocity zero points agree within 0.5 km s^{-1} between the two studies, with no apparent systematic offset. Given our higher resolution (by a factor $\sim$4), we can discern additional components toward γ Cas and δ Per; the statistics of component width and separation determined from the present survey (discussed below) suggest that additional unresolved component structure is likely to be present in a number of the other stars in the Welsh et al. sample. Finally, a plausible uncertainty in their instrumental FWHM of 0.1 km s^{-1} would imply uncertainties in their derived b-values of 0.15–0.28 and 0.08–0.10 km s^{-1}, for $b = 0.4$ and 0.8 km s^{-1}, respectively, so that our derived b-values should be much more reliable for $b \lesssim 1$ km s^{-1}.

3.4. *Parameter Statistics*

Of the 276 individual interstellar cloud components listed in Table 2, 38 have b-values that were essentially arbitrarily (though not unreasonably) fixed in the profile fitting. The

remaining 238 clouds constitute our primary sample for determining the statistics of various component parameters. The sample does reflect some selection biases—many of the lines of sight were chosen for having at least some relatively narrow, isolated components (though most such lines of sight also had additional components which did not meet those criteria), and the use of Na I introduces a bias toward the colder, denser clouds where Na I is most likely to be found. It is also possible that some of the absorption components are due to circumstellar, rather than interstellar material (see the discussion of o And in § 5.2 below). The sample also is probably not a full enumeration of the clouds producing detectable Na I absorption along the 38 lines of sight, as will be discussed below (§ 4.2.3). Although the derived component structures thus may not be absolutely correct in some individual cases, the total sample of "individual" interstellar clouds presented in Table 2 is both larger and likely more complete than most previous such samples (due to the very high resolution and relatively high S/N achieved for our spectra), and it does allow significant improvements over previous efforts to determine the statistical characteristics of interstellar clouds (see § 4.2 below).

Figure 4 shows the distribution of column density (log N) versus line width parameter (b); Figures 5 and 6 show, respectively, the individual distributions of b and log N. The solid histogram line in Figure 5 refers to the primary sample (defined above); the dotted line in Figure 5 and the solid line in Figure 6 refer to the full sample. Two additional scales near the top of Figure 5 denote the maximum values of the temperature (T_{max}) and one-dimensional rms turbulent velocity ($v_{t\,max}$) allowed for a given value of $b = [(2kT/m) + 2v_t^2]^{1/2}$; a third scale shows v_t for an assumed representative temperature of 80 K. The dashed lines in Figure 5 mark the b-values corresponding to our instrumental resolution (FWHM), to the case where $(3)^{1/2} \times v_t$ equals the isothermal sound speed ($v_s \sim 0.7$ km s^{-1}) at $T = 80$ K, and to the typical resolutions of IMAPS (2 km s^{-1}; Jenkins et al. 1989) and of the *HST* GHRS echelle (3.5 km s^{-1}); note that FWHM $\sim 1.665 \times b$. Only six clouds with log $N > 12.8$ cm^{-2} and seven clouds with $b > 2.6$ km s^{-1} have been excluded from these figures.

Inspection of Figures 4 through 6 immediately yields a number of qualitative observations. First, log N and b do not seem to be correlated, at least for the ranges in N and b sampled here. A range in log N seems to be possible for most values of $b \lesssim 1.5$ km s^{-1}, and vice versa. The median b for the primary sample is 0.73 km s^{-1}, slightly larger than the value most often observed ($\sim$0.55 km s^{-1}); the median log N for the full sample is $\sim$11.09 cm^{-2}. The maximum possible value for the one-dimensional turbulent velocity v_t is typically 0.5 ± 0.3 km s^{-1}. The apparent lack of narrow ($b \lesssim 0.4$ km s^{-1}) components for log $N \gtrsim 11.6$ cm^{-2} is probably due to our inability to disentangle the multiple narrow components contributing to the stronger absorption features. That inability to resolve closely blended components may also contribute to the comparative dearth of weak components (log $N \lesssim 10.2$ cm^{-2}) for all b, though that value of log N is also close to the detection limit for our lower S/N spectra. The median values of b and

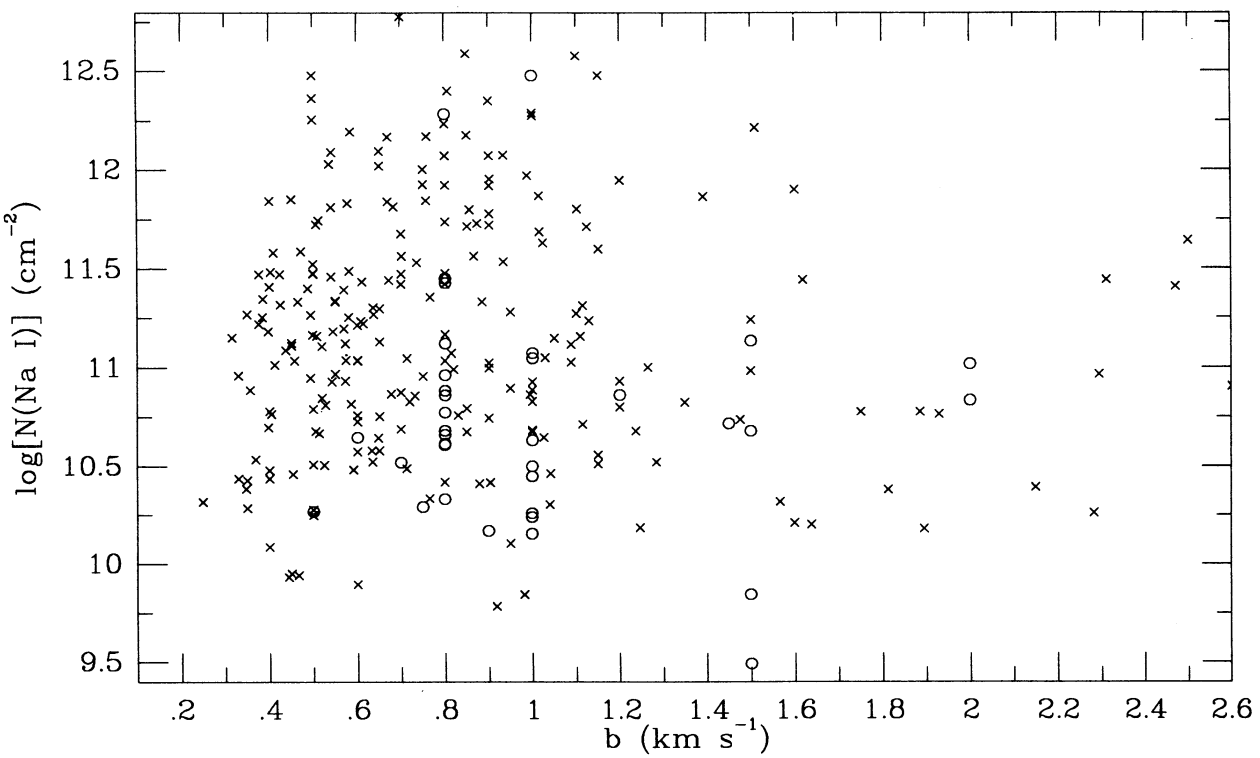

FIG. 4.—The distribution of log N(Na I) vs. b for the individual cloud components determined in the profile fits. An "o" indicates that b was fixed somewhat arbitrarily in the fitting; an "×" indicates that b was either varied or else fixed, but well determined. Only six points with log $N > 12.8$ cm^{-2} and seven points with $b > 2.6$ km s^{-1} are not included. Typical formal 1 σ errors in b range from a few hundredths of a km s^{-1} for narrow and/or relatively isolated lines to 0.1–0.3 km s^{-1} for wider and/or more blended lines. Corresponding errors in log N are less than 0.1 (dex) in nearly all cases, and are usually substantially less than that. There is no apparent correlation of the two parameters; the lack of points with $b \lesssim 0.6$ km s^{-1} for log $N \gtrsim 11.6$ cm^{-2} and with small log N for all b is likely due to the inability to resolve closely blended lines.

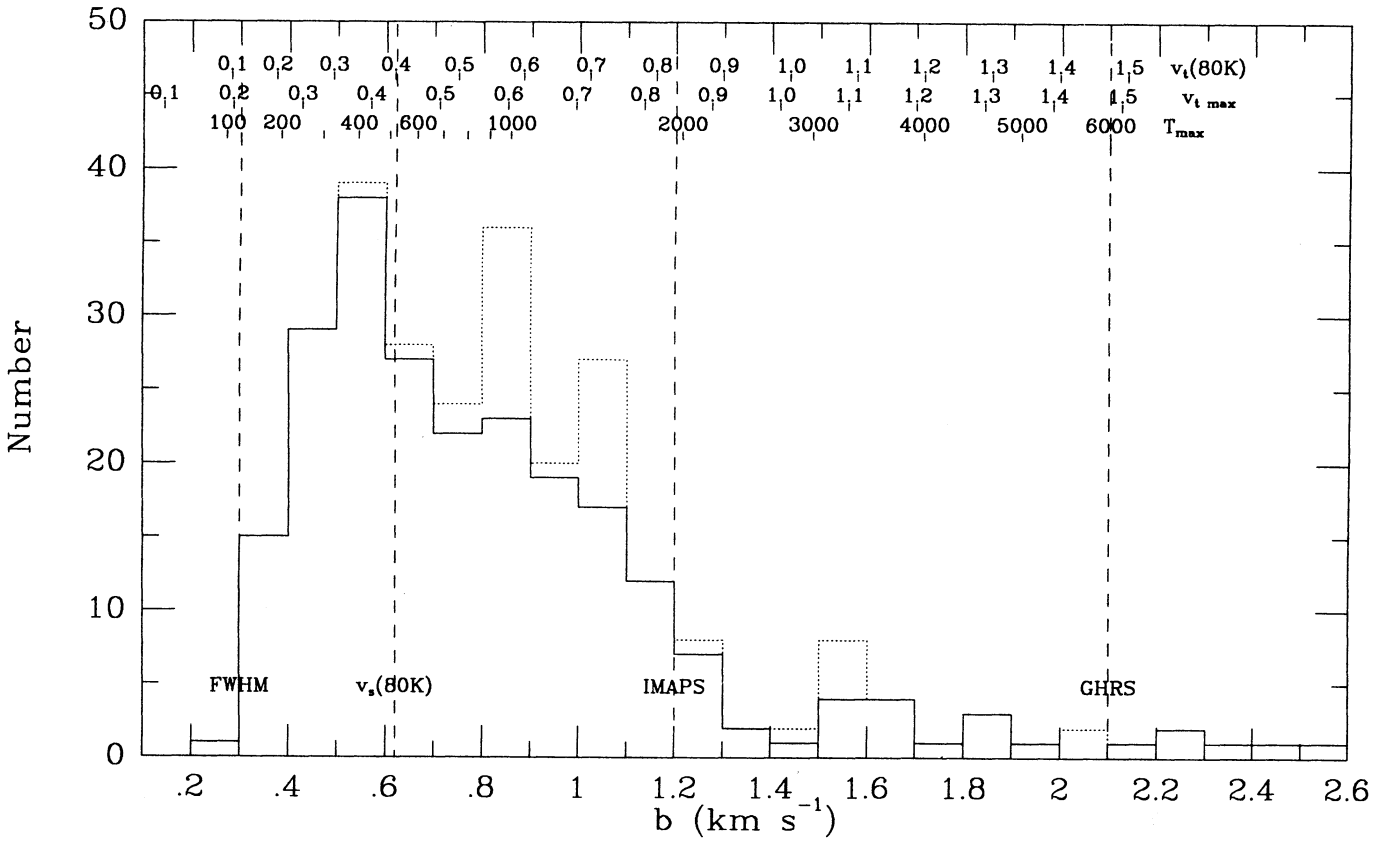

FIG. 5.—The distribution of the line width parameter b for the individual cloud components determined in the profile fits. The solid histogram corresponds to the primary sample of 238 clouds (both varied and fixed but well determined b); the dotted histogram corresponds to the full sample of 276 clouds (including the somewhat arbitrarily fixed, and thus less well-determined b). The additional scales at the top show the maximum temperature (T_{max}) and one-dimensional rms turbulent velocity $v_{t\,max}$ permitted for a given value of b, as well as the v_t for a "representative" temperature of 80 K. The dashed lines show the b-values corresponding to the instrumental resolutions (FWHM) of this study, of IMAPS, and of the *HST* GHRS echelle, and to a Na I absorption line having $(3)^{1/2} \times v_t$ equal to the isothermal sound speed ($v_s = 0.7$ km s^{-1}) at $T = 80$ K. The median b-value for the primary sample is 0.73 km s^{-1}; the number of b-values below 0.4 km s^{-1} is likely underestimated, however, due to our inability to resolve some narrow, closely spaced blends, so that the true median is likely somewhat lower. It will thus be difficult for either IMAPS or the GHRS to determine reliable b-values for many interstellar clouds. At least 38% (and likely a majority) of the clouds in the primary sample are characterized by subsonic internal turbulent motions if $T \sim 80$ K; the fraction will be higher if some clouds are warmer.

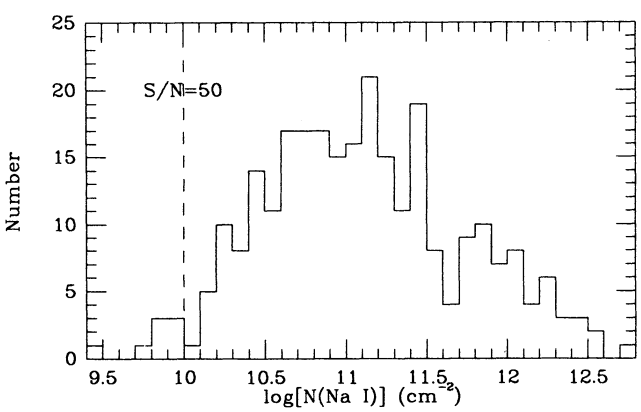

FIG. 6.—The distribution of log N(Na I) for the individual cloud components determined in the profile fits, for the full sample of 276 clouds. The median log N is 11.09 cm^{-2}; the number of weaker components has likely been underestimated, due to unresolved blends and to our detection limits, however, so that the true median is likely somewhat lower. The dashed line notes the 2 σ detection limit for a narrow line at S/N $\sim$ 50.

log N noted above are thus likely to be overestimates of the true values.

Figure 7 shows the distribution of velocity differences between adjacent components. The range in δv plotted emphasizes the statistics of component separations on relatively short scales; an additional 23 values of δv, ranging from 5.0 to 19.5 km s^{-1}, are omitted from the top panel of the figure. More than 85% of the adjacent component separations are less than 4.0 km s^{-1}; the median observed separation for the full sample, 2.0 km s^{-1}, is likely an overestimate of the true median, because of unresolved blends. The unresolved structure present (particularly) in many of the stronger absorption features probably accounts for the apparent fall-off in the distribution for $\delta v \lesssim 1.0$ km s^{-1}. The dashed lines indicate the resolutions (FWHM) achieved in this study, by IMAPS, and by the *HST* GHRS echelle; we also note the magnitude of the hyperfine splitting.

4. DISCUSSION

4.1. *Need for High Resolution*

Although the many strong absorption lines due to dominant neutral and singly ionized species present in the UV allow the detection of neutral interstellar clouds with much smaller total

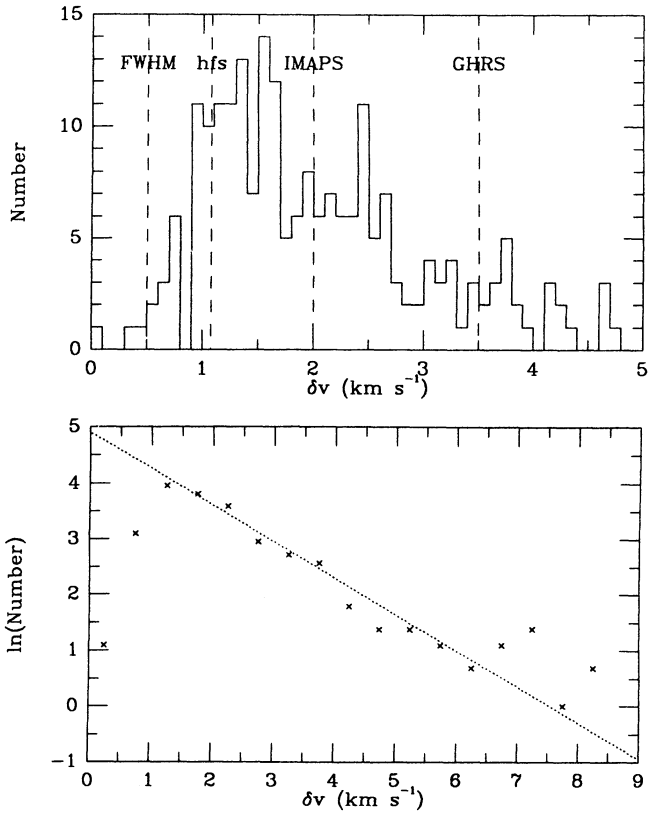

FIG. 7.—The distribution of the separation between adjacent components as determined in the profile fits, for the full sample of 238 differences; 23 points with $\delta v \gtrsim 5.0$ km s^{-1} are not included in the linear histogram at the top. The dashed lines mark the instrumental resolutions (FWHM) of this study, of IMAPS, and of the *HST* GHRS echelle; the latter two will be unable to resolve much of the structure seen in here in Na I. The magnitude of the Na I hyperfine splitting is also marked. More than 85% of the separations are less than 4.0 km s^{-1}; the median separation for the full sample, 2.0 km s^{-1}, is likely an overestimate. The logarithmic plot at the bottom shows that the distribution of separations (binned by 0.5 km s^{-1}) is well fitted by an exponential (*dotted line*), as would be expected for uncorrelated component velocities, between about 1.0 and 6.0 km s^{-1}. The falloff in the distribution below about 1.0 km s^{-1} indicates that we have not resolved most of the component blends with $\delta v \lesssim 1.0$ km s^{-1}; we may have detected only about 60% of the true total number of individual clouds above our detection limit along these lines of sight. The enhanced "tail" above about 6.0 km s^{-1} indicates that the underlying distribution of component velocities is more complex than a single Gaussian.

hydrogen column densities than is possible with the lines available in the optical, no UV spectrograph has had sufficient resolution to discern the detailed component structure seen in these Na I spectra. The *b*-values inferred from curve of growth abundance analyses of lower resolution (15–25 km s^{-1}) UV spectra are typically greater than 3 km s^{-1} (e.g., Jenkins, Savage, & Spitzer's 1986 *Copernicus* survey), and must generally reflect the velocity spread of multiple components along the various lines of sight rather than individual cloud absorption-line widths. While the resulting total line of sight abundances can be reasonably accurate (Jenkins 1986), most component to component variations would not be discernible. Even the detailed profile analyses of high S/N *Copernicus* data that make use of multiple transitions (e.g., Ferlet et al. 1980; Martin 1981; Martin & York 1982) cannot, in general, distinguish individual interstellar clouds; the derived *b*-values (often 2–3 km s^{-1}) and the derived component separations (usually 6–10 km s^{-1}) seem more representative of the component blends seen here in Na I. We note that there is considerable overlap between the lines of sight inclued in this Na I study and in the UV studies referenced above.

With accurate knowledge of the relevant instrumental profile and with high S/N spectra, one can obtain reliable *b*-values to perhaps one-fourth the instrumental FWHM when the component structure is well determined; with multiple transitions and sufficiently well-determined wavelengths, one can discern subcomponent structure to perhaps $\frac{1}{3}$ the FWHM. Thus even the *HST* GHRS echelle (FWHM ~ 3.5 km s^{-1}; wavelength uncertainties $\gtrsim 1$ km s^{-1}) would not be able to discern much of the component structure present in this Na I sample, nor would it allow accurate individual line widths to be determined in most cases. IMAPS (FWHM ~ 2 km s^{-1}) will do somewhat better, if higher S/N can be achieved, but will also fail to discern and characterize the narrowest, most blended components. Comparison of our D_1 profile toward γ Cas with that of Welsh et al. (1990), the latter obtained at 2 km s^{-1} resolution and high S/N, provides a particularly instructive illustration—Welsh et al. fit two components to their D_1 and D_2 spectra, but at least five are discernible in our D_1 spectrum shown in Figure 2. Jenkins et al. (1989) and Joseph & Jenkins (1991) were able to infer the presence of unresolved component structure from IMAPS spectra of π Sco, but could not determine column densities, *b*-values, or velocities for the individual components. Of course, both the GHRS and IMAPS should accurately characterize components that are both relatively isolated and intrinsically broad (i.e., warm and/or turbulent), as may be the case for much of the (halo) gas toward HD 93521 (Spitzer & Fitzpatrick 1993) and perhaps for clouds in the very local interstellar medium (e.g., Bertin et al. 1993). We note, however, that narrow, closely spaced Na I components seem to be common and ubiquitous; they apparently can be present both in halo lines of sight (e.g., ρ Leo; SN 1987A [Pettini 1988]) and toward relatively nearby stars (e.g., δ Cyg, 2 And), as well as toward more distant disk stars. "Individual component" comparisons of column densities, *b*-values, and velocities, as well as attempts to apply shock models to various lines of sight by identifying pre- and post-shock components, must be viewed with some caution, when the relevant spectra have been obtained at resolutions poorer than about 1 km s^{-1} (see also Black & van Dishoeck 1988).

It is clear from Figures 4–7 that high-resolution ($\lesssim 1$ km s^{-1}) observations of multiple transitions spanning a range of strengths will be needed for detailed understanding of the neutral interstellar medium along most lines of sight. For example, new high-resolution (0.3–1.2 km s^{-1}) spectra of the Ca II K line have recently been obtained for many of these lines of sight (Welty et al. 1994b). While there is good correspondence between a fair fraction of the (independently fitted) Na I and Ca II components, there are numerous cases where the lack of good correspondence may indicate the presence of still unresolved component structure in one or both of the species. Comparisons of the Na I and Ca II data with GHRS echelle spectra, for a few of these lines of sight, seem to indicate good agreement between (1) the relative abundances of Na I and other trace neutral species such as Mg I, S I, Fe I, and Si I; and (2) the relative abundances of Ca II and some of the dominant ionization states of depleted elements (e.g., Fe II, Ni II, Cr II, and Si II); within the uncertainties due to the lower resolution and S/N of the GHRS spectra (Lauroesch et al. 1994; Welty et al. 1994a). The use of very high resolution optical spectra to define the underlying component structure and the application of

profile analysis techniques to IMAPS and GHRS echelle spectra may thus (finally) yield reliable information about the properties (and variations thereof) of many individual interstellar clouds.

4.2. *Statistical Properties of Interstellar Clouds*

Maps derived from the emission observed from different constituents of the interstellar medium such as dust (*IRAS*) and various molecules (e.g., ^{12}CO and its isotopomers) reveal a complex, hieracrchical structure on all scales yet explored (e.g., Scalo 1990). Condensations are found embedded in filaments and sheets, which are in turn embedded in more tenuous material; temperature gradients must exist—the traditional picture of "standard" spherical, isothermal clouds would seem to bear little semblance to such observations. The multiple, blended components found (and suspected) in this survey at high spectral resolution and S/N—especially for higher column density features—may be a further manifestation of that complexity. Nonetheless, the absorption-line (and emission-line) data in many cases do reveal more or less separable features which can be described by a few parameters such as line width, column density, and line position; the statistics of these parameters, for large enough samples and for several different tracers, should provide useful constraints which would need to be satisfied by models of the interstellar medium.

4.2.1. *Component Velocity Distribution*

The observed shape and dispersion of the distribution of interstellar cloud velocities, with respect to the appropriate local standard of rest (LSR), can provide constraints for dynamical models of the interstellar medium. Spitzer (1968) has summarized early attempts, using 21 cm and low-resolution optical absorption-line data, to determine the cloud velocity distribution. Falgarone & Lequeux (1973) used both 21 cm absorption data and the high-resolution Na I spectra of Hobbs (1969a) to derive an overall one-dimensional velocity dispersion of 6.4 km s^{-1}, consistent with its value for several ranges in galactic latitude and D-line strength. Dickey, Salpeter, & Terzian (1978), from a sample of 66 H I 21 cm absorption components, found both an excess of negative velocity components at both high and low latitudes and a larger velocity dispersion for the weaker components.

In Figure 8, we show the distribution of log [N(Na I)] versus v_{LSR} for 270 of the 276 clouds in our full sample; values of the mean velocity $\langle v \rangle$ and of the dispersion $\langle v^2 \rangle^{1/2}$ are given in Table 3 along with similar results from Falgarone & Lequeux and Dickey et al. Figure 9 shows the distribution of v_{LSR} for the full sample and for two ranges in log [N(Na I)]. The LSR velocities have been corrected for differential galactic rotation using $\Delta v = A \times d \times \sin(2l) \times \cos^2(b)$, where we have used 15 km s^{-1} kpc^{-1} for Oort's constant A and have assumed a cloud distance d of half the distance to the star for each line of sight. We note that the mean and dispersion for the subsample of stars closer than 500 pc (chosen to minimize possible errors in the correction for differential galactic rotation and for comparison with Falgarone & Lequeux's values) are only slightly smaller than those for the full sample. The break point at log [N(Na I)] = 11.3 cm^{-2} between "large" and "small" clouds in Table 3 and Figure 9, chosen by inspection of Figure 8, corresponds to log [N(H I)] $\sim$ 20.1 $\pm$ 0.5 cm^{-2} (Ferlet, Vidal-Madjar, & Gry 1985; see § 4.3 below); Dickey et al.'s division at $(1 - e^{-\tau}) = 0.1$ corresponds to log [N(H I)] $\sim$ 19.85 cm^{-2}

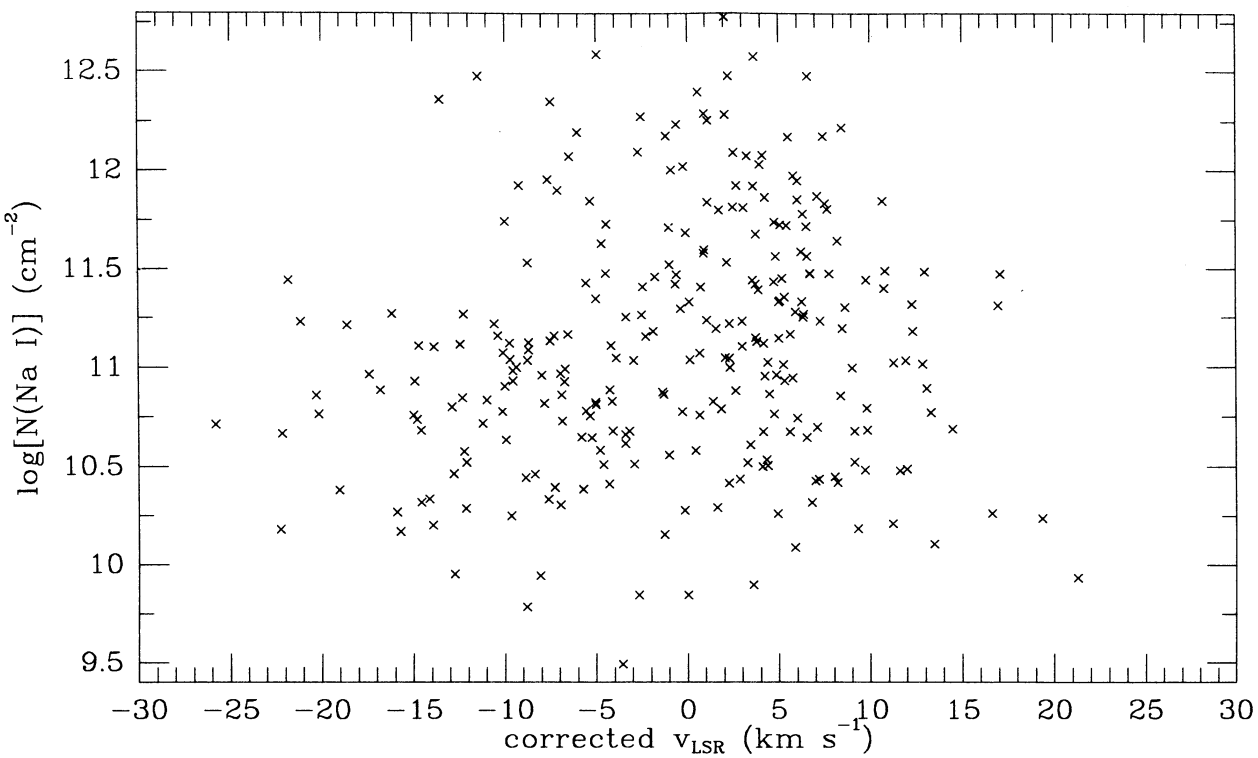

FIG. 8.—The distribution of log N(Na I) vs. v_{LSR} for the individual cloud components determined in the profile fits. The velocities have been corrected for differential galactic rotation assuming the clouds to be at half the distance to the stars. The mean velocity for the full sample is ~ -0.7 km s^{-1}; the velocity dispersion for the full sample is 8.6 km s^{-1}. The distribution of velocities is both broader and shifted to more negative velocities for the weaker components.

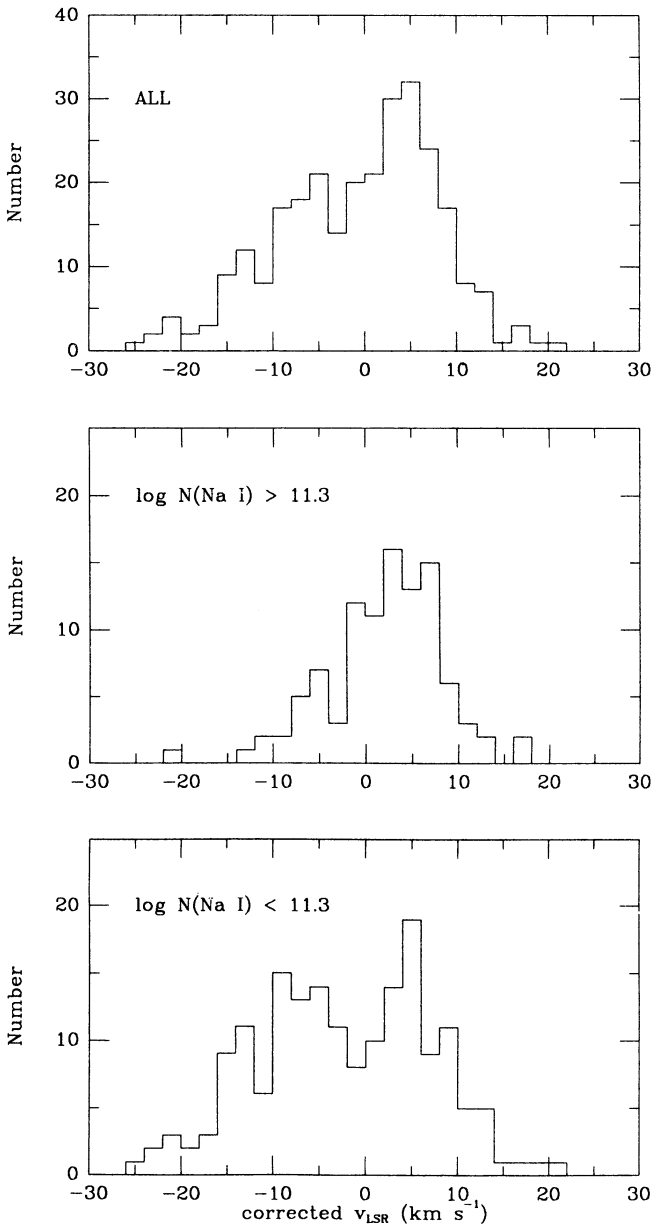

FIG. 9.—The distribution of component velocities, with respect to the local standard of rest and corrected approximately for differential galactic rotation. At the top is the distribution for the full sample; in the middle is the distribution for the components with log [N(Na I)] > 11.3 cm^{-2}; at the bottom is the distribution for the components with log [N(Na I)] < 11.3 cm^{-2}. The distribution of the stronger components is both narrower and centered at slightly more positive velocity, compared to the distribution of the weaker components.

(Payne, Salpeter, & Terzian 1983); Falgarone & Lequeux's limits on $\tau(D_2) > 0.2$ and 0.6 correspond to log [N(Na I)] $\gtrsim$ 10.6 and 11.1 cm^{-2}.

In agreement with Dickey et al., we find that the larger clouds have a slightly larger mean velocity and a significantly smaller velocity dispersion than the smaller clouds. While the asymmetric tail to negative velocities (due primarily to the smaller clouds) seen in Figure 9 could suggest that those clouds are associated with and accelerated by the mostly early type stars in our sample, that would not explain the concordant result from Dickey et al.'s 21 cm sample, The exact numbers for

TABLE 3

LSR VELOCITY DISTRIBUTIONS

Data Set[1]	#	$\langle v \rangle$ (km s^{-1})	$\langle v^2 \rangle^{1/2}$ (km s^{-1})
Na I (all stars)			
log N > 11.3	101	2.06	6.59
log N < 11.3	175	-2.29	9.57
all components	276	-0.70	8.60
Na I (d $\leq$ 500 pc)			
log N > 11.3	84	1.66	6.43
log N < 11.3	143	-1.80	9.00
all components	227	-0.52	8.14
H I (DST 1978)			
$(1 - e^{-\tau}) > 0.1$	36	0.95	5.3
$(1 - e^{-\tau}) < 0.1$	30	-2.72	11.5
all components	66	-0.72	8.7
H I (FL 1973)			
$\lvert b \rvert > 15$	...	...	6.4
$\lvert b \rvert > 34$	...	...	5.8
$15 < \lvert b \rvert < 34$	...	...	6.9
Na I (FL 1973)			
$\tau(D_2) > 0.2$	...	...	6.9
$\tau(D_2) > 0.6$	...	...	5.9

[1] DST 1978: Dickey et al. 1978. FL 1973: Falgarone & Lequeux 1973.

$\langle v \rangle$ and $\langle v^2 \rangle^{1/2}$ are dependent both on the set of lines of sight chosen and on the range of cloud column densities included; our values are somewhat higher than those derived for Na I by Falgarone & Lequeux because we observed more of the more complex lines of sight in the Hobbs (1969a) sample and also because our velocity coverage was somewhat better (enabling more reliable detection of weak, outlying components). The probable incompleteness of our sample suggests that our values for $\langle v^2 \rangle^{1/2}$ are overestimates of the true values, as most of the additional missed components are likely to be hidden in the stronger components at relatively low $\lvert v_{LSR} \rvert$.

4.2.2. *Line Widths*

The widths of individual absorption (or emission) features can yield information concerning the temperature and internal motions in the corresponding interstellar clouds—with significant implications for the chemistry and energetics. For lines of comparable strength, comparison of two species with similar atomic weight can yield information on their relative spatial distribution, while comparison of two (assumed) coexistent species of different atomic weight can allow some measure of the temperature and internal turbulent motions to be separately determined. Radio observations of various molecular emission lines offer the advantages of very high resolution (e.g., $R \gtrsim 10^7$ for recent observations of HC_3N by Fuller & Myers 1993) and spatial mapping, but can typically probe only the coldest, densest regions; the different beam sizes used for different species can also make comparisons difficult. Absorption-line observations can probe more diffuse objects, with the same (very small) beam size; most existing data do not have the required high spectral resolution and/or S/N to reliably isolate distinct individual components, however.

Payne et al. (1983) have analyzed sensitive H I 21 cm emission/absorption data obtained with the Arecibo radio telescope at a resolution of 0.25–0.50 km s^{-1} for a number of lines of sight at $b \gtrsim 5°$. They decomposed the derived absorption profiles into Gaussian components, then examined the statistical properties of the resulting sample of interstellar clouds, each characterized by a maximum optical depth τ_{max}, a corresponding harmonic mean temperature T_{min} corrected for "not strongly absorbing" gas, an observed FWHM, and a "nominal" column density N. For 50 clouds with $0.02 \lesssim \tau_{max} \lesssim 1.0$, they found (1) $T_{min} = (55 \pm 7\ \mathrm{K}) \times [1 - \exp(-\tau_{max})]^{-(0.34 \pm 0.05)}$, with a scatter of about a factor 2; (2) $\mathrm{FWHM_{obs}} \sim (1.3 \pm 0.5) \times \mathrm{FWHM_{thermal}}$, independent of τ_{max}; and (3) the probability of observing N greater than some N_c is proportional to $N_c^{-0.82}$. As discussed by Heiles & Kulkarni (1987), the median cloud in the sample has $\tau_{max} = 0.07$, $T_{min} = 135$ K, and $N = 0.6 \times 10^{20}$ cm^{-2}; the limits on τ_{max} correspond to 0.32×10^{20} cm$^{-2} \lesssim N \lesssim 2.2 \times 10^{20}$ cm^{-2} and 208 K $\gtrsim T_{min} \gtrsim$ 64 K. For that range in temperature, we can further derive 1.9 km s$^{-1} \gtrsim b_{thermal} \gtrsim 1.0$ km s^{-1}, 4.0 km s$^{-1} \gtrsim \mathrm{FWHM_{obs}} \gtrsim 2.3$ km s^{-1}, and thus 1.0 km s$^{-1} \gtrsim v_t \gtrsim$ 0.6 km s^{-1}. If Na I and H I are characterized by the same temperature and turbulent velocity in these clouds, then for Na I we would have 0.4 km s$^{-1} \gtrsim b_{thermal} \gtrsim 0.2$ km s^{-1} and 1.5 km s$^{-1} \gtrsim b_{total} \gtrsim 0.9$ km s^{-1}. The H I line widths would be dominated by thermal broadening, while the Na I line widths would be strongly dominated by internal turbulent motions. We note, however, that both the FWHM and the component separations derived in Payne et al.'s Gaussian decomposition of their H I profiles are larger than the typical line separations found in this Na I study, and that the predicted Na I b-values are larger than most of those measured in our spectra. Our observed median log [N(Na I)], likely an upper limit to the true median, corresponds to log [$N(\mathrm{H_{tot}})$] of 19.9 ± 0.5 cm^{-2} (Ferlet et al. 1985), and may be consistent with the median log [N(H I)] ~ 19.8 cm^{-2} determined by Payne et al.

The differences in cloud properties as determined from H I and Na I observations are likely due to a combination of two effects. Part of the difference in the widths of the H I and Na I components may be due to differences in the spatial distribution of the two species. Since Na I is a trace ionization stage in H I regions, its abundance is proportional to the square of the local hydrogen density, and thus it will be concentrated in the colder, denser portions of the clouds. The H I will typically be more extensively distributed than the Na I; the larger H I line widths might thus reflect an increased range of turbulence and/or a higher average temperature in that larger region. In addition, we suspect that the large thermal broadening for H I, due to its small atomic weight, may have hidden significant subcomponent structure in the H I absorption profiles analyzed by Payne et al., even though their resolution was somewhat better than that achieved in this Na I study. If the H I absorption profiles contain unresolved substructure, then both the FWHM and the turbulent contribution to the H I line widths derived from Payne et al.'s absorption-line profile fits will have been overestimated. Since the widths of H I emission lines are typically larger than those of the corresponding absorption lines, (likely) due to temperature variations and the larger effective beam size for the emission observations (e.g., Liszt 1983), attempts to derive component structures from 21 cm emission profiles would be even more severely affected. The presence of unrecognized substructure in the H I profiles would also imply that the distribution of H I column densities is actually steeper than $N^{-0.82}$. Deriving an H I column density distribution from our Na I data, however, would require a better knowledge of the ratio of the two species than is currently available (see § 4.3 below).

Hobbs (1974b) presented distributions in b and N for 37 clouds seen in K I absorption, observed at a resolution of about 1.2 km s^{-1}, along 17 lines of sight. For that sample, he found a mean b of 1.48 km s^{-1} and a mean log [N(K I)] of about 11.3 cm^{-2}. A number of the "single" clouds in that sample can now be shown to consist of at least two closely blended components, however, so that the true mean b will be significantly smaller than 1.48 km s^{-1} (Welty et al. 1994b). Furthermore, if we assume a typical ratio of Na I to K I of about 70 (Welty et al. 1991), the mean K I column density corresponds to a mean log [N(Na I)] ~ 13.1, two orders of magnitude larger than the median log [N(Na I)] found here, so that the K I sample does not represent the majority of interstellar clouds (as noted also by Heiles & Kulkarni 1987).

Due to the apparently widespread presence of narrow, closely blended components and the likelihood that different species trace different physical regions, determination of the "true" distributions of T, v_t, and N for individual interstellar clouds will require observations of a set of species sensitive to different ranges of $N(\mathrm{H_{tot}}) = N(\mathrm{H\ I}) + 2N(\mathrm{H_2})$—all at resolutions comparable to or better than that achieved in this study. For the small set of dense cores examined by Fuller & Myers (1993), comparison of emission-line widths from the apparently similarly located HC_3N (0.08 km s$^{-1} \lesssim b \lesssim$ 0.21 km s^{-1}) and NH_3 (0.12 km s$^{-1} \lesssim b \lesssim$ 0.27 km s^{-1}) implies that the widths are dominated by thermal broadening (at $T \lesssim 10$ K), with a minor nonthermal (turbulent) contribution. Myers (1983) had previously found turbulent velocities to be subsonic in the small, dense cores traced by NH_3, but often supersonic in the larger regions traced by CO (assuming $T \sim 10$ K, so that $v_s \sim 0.2$ km s^{-1}). For the denser parts of translucent ($1 \lesssim A_V \lesssim 5$) and diffuse ($A_V \lesssim 1$) clouds, observations of various rotational transitions of C_2 and H_2 indicate temperatures ranging from 15 to 55 K (Black & van Dishoeck 1991) and 45 to 128 K (Savage et al. 1977), respectively. High-resolution observations of ^{13}CO emission-line widths (e.g., Gredel, van Dishoeck, & Black 1991) and CN absorption-line widths (ζ Oph; Lambert et al. 1990), as well as comparisons of the B–X (0, 0) and A–X (2, 0) bands of CN (Gredel et al. 1991), imply 0.3 km s$^{-1} \lesssim b \lesssim 1.0$ km s^{-1} for those species in such clouds. While a few of the clouds listed in Table 2 would qualify as "translucent," most of them are more diffuse; the range of b-values for Na I is quite similar to that seen for the denser regions traced by CN and CO, however. If the temperatures noted above are accurate and applicable to these species, the narrower lines in these clouds would be dominated by thermal broadening, but the wider lines would be dominated by internal turbulent broadening.

Nineteen of the lines of sight in our sample appear in the Savage et al. (1977) H_2 survey; 11 of those have $J = 0$ and $J = 1$ column densities greater than 10^{18} cm^{-2}, with implied temperatures between 46 and 92 K. If we take 80 K as a representative temperature for all the individual clouds in our survey and assume that $N(\mathrm{H_2})/N(\mathrm{H\ I})$ is small, then $(3)^{1/2} \times v_t$, typically 0.9 ± 0.5 km s^{-1}, would be subsonic (i.e., $\lesssim$0.7 km s^{-1}) in at least 38% of the clouds. Since we have probably underestimated the number of narrow components, and since the temperatures of the lower column density clouds are likely to be somewhat higher than 80 K, it is likely that the majority

of the clouds seen in Na I have subsonic internal turbulent motions. High-resolution, high S/N observations of Ca II and K I, heavier than Na I by nearly a factor of 2, would be quite valuable in assessing the relative contributions of thermal and turbulent broadening in these lines of sight.

4.2.3. *Sample Completeness*

We have already mentioned several reasons to suspect that our derived Na I component structures may not include all the Na I components actually present. We may have missed some very broad, weak components either in performing the continuum normalization or in the fitting, if any such components might be superposed on blends of narrower lines. Conversely, some broad features are probably blends of narrower components; the broad components seen toward o^2 CMa, for example, are likely due to the blending of a number of narrower components by differential galactic rotation along that line of sight. In addition, our inability to adequately fit some of the stronger Na I lines indicates that we have not resolved all the component structure present in those stronger absorption features. This conclusion is supported in several cases by high-resolution spectra of Ca II and/or K I which do reveal additional structure that is unresolved in the stronger Na I lines. Additional weak and/or narrow absorption components, which can be clearly seen in isolation or on the peripheries of stronger features, may be present as well within the stronger features.

The apparent falloff in the distribution of adjacent component separations for $\delta v \lesssim 1.0$ km s^{-1} in Figure 7 is another indication of unresolved structure; this distribution also provides a way of estimating the degree to which our sample may be incomplete. If the component velocities for the true complete sample of clouds are both uncorrelated and taken from a single Poisson distribution, then the distribution of adjacent component separations will be an exponential function of δv. In practice, a number of other velocity distributions will also yield a distribution of adjacent component separations that can be approximated by an exponential over some range $\delta v \lesssim \delta v_{max}$, though some velocity distributions (e.g., narrow Gaussian plus broad Gaussian, or exponential) will give an enhanced "tail" for $\delta v \gtrsim \delta v_{max}$. The observed distribution of adjacent component separations does appear to have such a tail for $\delta v \gtrsim 6.0$ km s^{-1} (see the plot of ln [number] vs. ∂v in the lower panel of Fig. 7), but it can be reasonably well fitted by an exponential for 1.0 km s^{-1} $\leq \delta v \lesssim$ 4.0–6.0 km s^{-1}, with ln (number) $\sim(4.9 \pm 0.1)$–$(0.65 \pm 0.05) \times \delta v$ (binning by 0.5 km s^{-1} in δv). If we extrapolate that best-fit exponential to $\delta v = 0.0$ km s^{-1}, we would predict $\sim$390 components for $\delta v \leq 6.0$ km s^{-1}, instead of the $\sim$220 observed in that range—with the difference mostly at $\delta v \lesssim 1.0$ km s^{-1}. The 276 components in our full sample would thus represent only about 60% of the true complete sample of clouds which could have been detected along these 38 lines of sight. The true median δv would then be $\sim$1.2–1.3 km s^{-1} (instead of 2.0 km s^{-1}); we cannot estimate the corresponding true median values for b and log [N(Na I)], but suspect that they would also be smaller than their values for the 276 cloud sample. If we divide the total number of components by the total distance to all 38 stars in our sample, we obtain 20 (33) components per kpc for 276 (446) total components. It is rather sobering to consider that at a resolution of 0.5 km s^{-1} we may have failed to discern 40% of the components present above our detection limit—or more, if the true distribution of component separations is actually steeper for $\delta v \lesssim 6.0$ km s^{-1}.

4.3. *Ratio of* Na I *to* H_{tot}

Since it is easier in many cases to obtain accurate values for N(Na I) than for $N(H_{tot})$, especially for individual clouds, it is of some interest to examine the relationship between the two quantities; N(Na I) has been used to estimate $N(H_{tot})$ when the latter is unavailable (though see the criticism of Heiles & Kulkarni 1987). Hobbs (1974a; 1976) and Stokes (1978) both found a roughly quadratic relation between N(Na I) and $N(H_{tot})$, for 11.3 cm^{-2} $\lesssim$ log [N(Na I)] $\lesssim$ 13.9 cm^{-2} and 20.2 cm^{-2} $\lesssim$ log [$N(H_{tot})$] $\lesssim$ 21.4 cm^{-2}, with a scatter of about a factor of 2. Hobbs interpreted that relation to imply a statistically constant fractional ionization n_e/n_H in the clouds observed. Ferlet et al. (1985) extended the comparison of the two species to lower limits (log [N(Na I)] $\sim$ 10.0 cm^{-2}; log [$N(H_{tot})$] $\sim$ 18.0 cm^{-2}) by observing weak Na I lines and by inferring $N(H_{tot})$ from profile analyses of high S/N UV data from *Copernicus*. For higher column densities (log [$N(H_{tot})$] $\gtrsim$ 21.0 cm^{-2}), Ferlet et al. also found a roughly quadratic relation; for lower column densities, however, they found a nearly linear relation, which they interpreted as indicating a more or less constant product of the Na recombination coefficient (α) and the local electron density (n_e) for the lower column density clouds. The lowest column density regime (log [$N(H_{tot})$] $\lesssim$ 19.0 cm^{-2}), however, was defined by only five points, at least three of which can now be shown to be inaccurately located: ζ Oph (-28 km s^{-1}) has N(H) higher by a factor of 7 (Savage, Cardelli, & Sofia 1992), ϵ Per ($+19$ km s^{-1}) has N(Na I) lower by a factor of 2, and γ Cas ($+6$ km s^{-1}) has N(Na I) lower by at last a factor of 3 (it may be completely spurious). Column densities for Na I (Crawford 1991; Centurion & Vladilo 1991), for H I (Bohlin et al. 1983; Diplas & Savage 1994), and for O I and N I (York et al. 1983) are now available for additional lines of sight with log [N(Na I)] $\lesssim$ 11.0 cm^{-2}. These data indicate an increasing range of N(H I) for a given N(Na I) as the latter decreases, reaching roughly two orders of magnitude for log [N(Na I)] $\sim$ 10.0 cm^{-2}. Furthermore, the Ferlet et al. linear relationship generally underestimates N(H I) for a given N(Na I) at these low column densities—by up to a factor $\sim$30 at log [N(Na I)] $\sim$ 10.0 cm^{-2}. Predictions of N(H I) based on observations of Na I must be viewed with caution when log [N(Na I)] $\lesssim$ 11.0 cm^{-2}. Additional observations are needed to better explore the H I–Na I relationship for the lower column densities; detailed, component by component comparisons of Na I with relatively undepleted species such as Zn II, S II, N I, and O I, observed with IMAPS and/or the *HST* GHRS echelle, will be quite useful.

5. INDIVIDUAL LINES OF SIGHT

5.1. *Local Interstellar Components toward Scorpius-Ophiuchus*

A number of stars in Upper Scorpius and Ophiuchus show Na I absorption components between roughly -23 and -29 km s^{-1}, in addition to the much stronger components found between -8 and -15 km s^{-1} (Fig. 2; Hobbs 1969a; Crawford 1991). Ultraviolet absorption-line data suggest that these weaker components at more negative velocity are characterized by significantly reduced depletions of the various refractory elements, similar to those found in higher velocity gas and lower average density lines of sight (Snow & Meyers 1979; Frisch 1981; Meyers et al. 1985; Savage et al. 1992). Frisch & York (1984) presented spectra for several stars within several degrees of ζ Oph at distances of 55–90 pc which implied that this gas is located within 80 pc; Frisch (1981) had conjectured that it might be much closer, based on comparisons with the

absorption seen toward α Oph (at ~20 pc). While this gas is usually thought to be warm (Frisch 1981; Joseph & Jenkins 1991; Savage et al. 1992), it is clear from Figures 2 and 3 and from Table 2 that there are at least several fairly cold components contributing toward ζ Oph and β^1 Sco. Some of the abundances in this gas, and ideas as to its history, may need to be reconsidered in light of the presence of these relatively cold components.

Toward α Oph, we find two weak, relatively broad components in Na I, separated by about 4.2 km s^{-1}, at velocities corresponding to Bertin et al.'s (1993) nearby clouds "G" and "LIC" (Local Interstellar Cloud), respectively. The component near −22.0 km s^{-1} was observed near 0.0 km s^{-1} geocentric velocity, and thus probably includes some telluric Na I absorption, but it is too broad and strong to be entirely telluric. Other high S/N spectra obtained on the same nights as the α Oph spectra indicate a likely telluric contribution to that component of about $(7 \pm 1) \times 10^9$ cm^{-2}, leaving $N_{\rm LIC} \sim (3 \pm 1) \times 10^9$ cm^{-2} near Bertin et al.'s predicted LIC velocity of −22.7 km s^{-1}. New high-resolution data for the stronger Ca II lines (Welty et al. 1994b) also require two components; the ratio N(Na I)/N(Ca II) is consistent with 0.1 for both. Although Bertin et al. fit a single component to their 3 km s^{-1} resolution Na I spectra of α Oph, their b-values are somewhat larger than ours, and they did conjecture that a second component might also be present; there, again, the issue is clouded by the probable presence of telluric Na I. Both components may be included in the −25 km s^{-1} H I "wisp" discussed by Frisch, York, & Fowler (1987), given its FWHM ~ 9 km s^{-1}. If that H I wisp corresponds mainly to the stronger component seen in Na I and Ca II, then its width sets an upper limit of $T \lesssim 1600$ K for that gas; the relatively large b-values found for both Na I D_1 (2.15 km s^{-1}) and Ca II (2.6 km s^{-1}) would be consistent with that limit if the lines are dominated by turbulent broadening.

5.2. *o And Shell Episode*

One of our four total observations of o And was obtained on 1987 October 28 during the onset of a shell phase (Peters 1988). That Na I spectrum is plotted in Figure 2 immediately below the sum of the other three (non–shell-phase) spectra of o And, with the fit to the latter superposed. While there seems to be a slight oversubtraction of the background for velocities greater than about −13 km s^{-1}, there is a clear excess of absorption between about −6 and −3 km s^{-1} which is presumably due to the shell.

5.3. *ε Ari A and MBM 12*

Observations of the strong Na I absorption toward ε Ari A have been used to constrain the distance to the high-latitude molecular cloud MBM 12 (Magnani, Blitz, & Mundy 1985). At $d \sim 65$ pc, MBM 12 is perhaps the nearest known molecular cloud, and may be at least partially immersed in the local hot bubble (Hobbs et al. 1986; Snowden, McCammon, & Verter 1993). The 11.5 km s^{-1} component is similar in velocity to the CO observed in the northern part of MBM 12 near ε Ari A (e.g., Zimmermann & Ungerechts 1990), and is likely due to atomic gas associated with the molecular cloud. While several other stars near MBM 12 also show absorption near 15.7 km s^{-1}, the association of this gas with the molecular cloud is not as obvious; see Fowler (1994) for a more complete discussion of the local interstellar medium in this region. The Na I lines are rather broad ($b \sim 1.5$ km s^{-1}), but we note that the CO lines in MBM 12 are also broad (1.1 km s$^{-1} \lesssim b \lesssim 1.6$ km s^{-1} in the northern part of the cloud) (Pound, Bania, & Wilson 1990; Zimmermann & Ungerechts 1990)—perhaps indicative of interaction with the hot gas thought to reside in the local bubble. Due to the low S/N of this Na I spectrum, and to the low resolution of the available Ca II data, we cannot at this time reliably estimate T and v_t in the clouds toward ε Ari A, however.

5.4. *η Tau, 17 Tau, 27 Tau, and the "Pleiades Wake"*

White & Bally (1993) have discussed the interaction between the Pleiades cluster and the interstellar gas through which the cluster is moving. Their picture of that interaction predicts that some cluster stars should show absorption components blue-shifted by ~10 km s^{-1} with respect to the main interstellar component seen at $v \sim 16$ km s^{-1}. In support of their interaction scenario, they cite a possible weak absorption component at $v \sim 5$ km s^{-1} in Welsh et al.'s (1991) Na I spectra of η Tau. We see no compelling evidence, at 2 σ equivalent width limits better than 1 mÅ, for absorption components near $v = 5$ km s^{-1} in our Na I spectra of η Tau, 17 Tau, or 27 Tau, though a very weak component might be present toward 27 Tau. We note, however, that an absorption component does appear at $v = 5$ km s^{-1} in Ca II spectra of η Tau (Vallerga et al. 1993; Welty et al. 1994b); Ca II will be a more sensitive tracer of shocked gas in which grains have been disrupted to some extent.

6. SUMMARY

We have obtained high-resolution (0.5 km s^{-1}) spectra of the interstellar Na I D_1 line toward 38 bright stars with the McDonald Observatory 2.7 m coudé echelle spectrograph. The S/N achieved in the final summed spectra is typically 45–280, yielding 2 σ equivalent width limits for narrow lines of about 0.2–1.0 mÅ, and corresponding Na I column density limits of 0.2–1.0 × 10^{10} cm^{-2}; the velocities, calibrated via I_2 absorption and Na emission spectra, are accurate to within about 0.3 km s^{-1}. Numerous narrow, closely blended components, which could not be distinguished in spectra obtained even at a resolution of 1.0 km s^{-1}, are evident in these new spectra, especially for the stronger absorption features. These narrow components, showing at least partially resolved hyperfine structure, are common and ubiquitous, appearing in both low halo and quite local gas, as well as in gas toward more distant disk stars.

We have used the method of profile fitting in an attempt to determine individual cloud column densities, line widths, and velocities; the resulting sample of 276 clouds is significantly larger, and likely more complete, than several previous samples of "individual" interstellar clouds, and allows more precise investigation of various statistical properties. We find that the cloud column density (N) and line width parameter (b) are not correlated, for 0.3 km s$^{-1} \lesssim b \lesssim 1.5$ km s^{-1} and 10.0 cm$^{-2} \lesssim \log [N(\text{Na I})] \lesssim 11.6$ cm^{-2}. The median b is about 0.73 km s^{-1}, the median log N is about 11.09 cm^{-2}, and the median separation between components is about 2.0 km s^{-1}. All these are overestimates of the true median values, however, due to our inability to completely resolve all the component structure present in some cases; even at a resolution of 0.5 km s^{-1}, we many have discerned only 60% of the full number of individual components actually present. Previous statistical studies are likely to have been even less complete, however, and probably have even more severely overestimated these parameters. The

one-dimensional dispersion of component velocities, in the local standard of rest, is approximately 8.6 km s^{-1}; the distribution of velocities is broader and displaced to more negative velocities for the weaker components. If most line widths lie in the range 0.3 km $s^{-1} \lesssim b \lesssim 1.1$ km s^{-1}, and if 80 K is a typical cloud temperature, then the one-dimensional rms turbulent velocity v_t is typically 0.5 ± 0.3 km s^{-1} and at least 38% (and probably a majority) of the clouds have subsonic rms internal turbulent motions. At that temperature, the narrower lines are dominated by thermal broadening, while the broader lines are dominated by turbulent broadening. Examination of existing column density data for Na I, H I, O I, and N I show that the range in N(H I) observed at a given N(Na I) increases as N(Na I) decreases below about 10^{11} cm^{-2}, so that N(Na I) becomes a much less reliable predictor of N(H I) at low Na I column densities.

These data will be quite useful for detailed studies of these lines of sight with the *HST* GHRS echelle—to determine accurate absolute velocities and to reveal the detailed component structures that cannot be discerned at the 3.5 km s^{-1} resolution achievable with the GHRS. By using very high resolution optical spectra to interpret the GHRS echelle spectra, it may be possible, in many cases, to obtain individual cloud column densities, line widths, and velocities for many of the species observable only in the UV, and thus to better understand the true range of interstellar cloud properties in different environments.

We are grateful to the staff at McDonald Observatory, and in particular David Doss, for their hospitality and expert assistance. We thank D. Willmarth and C. Plymate at KPNO for obtaining the high-resolution Th/Ar spectrum, and the referee for several fruitful suggestions. Alex Dalgarno kindly pointed out R. D. Cowan's book to us and reviewed Appendix A critically. Financial support for this work was provided via NASA grant NAGW-1475 to the University of Chicago.

APPENDIX A

The transition probabilities of the various lines constituting a hfs multiplet are proportional to the transition probability of the single, corresponding line which results when the hfs is ignored. In L-S coupling, the relative line strengths $S(i, j)$ of the various lines within a hfs multiplet which connect lower hfs levels with $F = i$ to upper levels with $F = j$ can be read, for example, from Table 1[9] of Condon & Shortley (1963), with the substitutions $L \rightarrow J$, $S \rightarrow I$, and $J \rightarrow F$. The normalization of these line strengths is fixed by the requirement that $\sum S(i, j) = (2I + 1)S$, where the sums extend over the hfs multiplet and S is the strength of the single, unresolved line obtained when the hfs is ignored. The full sum of the line strengths of the hfs multiplet exceeds the line strength of the unresolved line by the factor $(2I + 1)$ (Cowan 1981, eq. [17.63]). For any transition with an oscillator strength f and a statistical weight g in the lower level, S is proportional to $gf\lambda$. If the wavelength differences among members of a hfs multiplet are negligibly small, as is normally true, a simpler approximation to the normalization condition therefore is that $\sum g_i f(i, j) \sim (2I + 1)gf$, where the product gf refers to the entirely unresolved line.

As the example which is applicable here, consider the Na I D_1 line, for which the lower and upper electronic levels are $3s^2S_{1/2}$ and $3p^2P_{1/2}$, respectively, and for which the nuclear spin is $I = 3/2$. The hyperfine interaction splits both electronic levels with $J = \frac{1}{2}$ into two hfs levels with $F = 1, 2$; the much smaller splitting of the upper levels is often negligible, in practice (McNutt & Mack 1963). In L-S coupling, the relative line strengths are found to be $S(1, 1)/S(1, 2)/S(2, 1)/S(2, 2) = 1/5/5/5$. If the statistical weights $g_F = 2F + 1$ are introduced, and if small wavelength differences are ignored, the ratios of the corresponding oscillator strengths are $f(1, 1)/f(1, 2)/f(2, 1)/f(2, 2) \sim 1/5/3/3$. The normalization is then fixed by the requirement that $g_1 f_1 + g_2 f_2 = g_1[f(1, 1) + f(1, 2)] + g_2[f(2, 1) + f(2, 2)] \sim (2I + 1)gf$, or $3f_1 + 5f_2 \sim 8f$, since $g_1 = 3$, $g_2 = 5$, and $g = 2$. In the L-S coupling limit, the final results therefore are that $f(1, 1) \sim f/6$, $f(1, 2) \sim 5f/6$, and $f(2, 1) = f(2, 2) \sim f/2$, where $f = 0.318$ for the unresolved D_1 line (Morton 1991). For the two s-resolved hfs components of the D_1 line which are actually of interest here, $f_1 = f_2 = f$ and $g_1 f_1 = 3f$, $g_2 f_2 = 5f$.

The Na I D_2 line has an upper $3p^2P_{3/2}$ electronic level which splits into $F = 0, 1, 2, 3$; the separations among these levels are often negligible in practice, as well. The relative strengths are $S(1, 0)/S(1, 1)/S(1, 2)/S(2, 1)/S(2, 2)/S(2, 3) = 2/5/5/1/5/14$, and $f(1, 0)/f(1, 1)/f(1, 2)/f(2, 1)/f(2, 2)/f(2, 3) \sim 10/25/25/3/15/42$, while the normalization condition is $3f_1 + 5f_2 = 3[f(1, 0) + f(1, 1) + f(1, 2)] + 5[f(2, 1) + f(2, 2) + f(2, 3)] \sim 8f$. In the L-S coupling limit, the results are that $f(1, 0) \sim f/6$, $f(1, 1) = f(1, 2) \sim 5f/12$, $f(2, 1) \sim f/20$, $f(2, 2) \sim f/4$, and $f(2, 3) \sim 7f/10$, where $f = 0.631$ for the unresolved D_2 line. Just as for the D_1 line, the two s-resolved hfs components of the D_2 line therefore show $f_1 = f_2 \sim f$ and $g_1 f_1 \sim 3f$, $g_2 f_2 \sim 5f$.

In passing, it should be noted that the sum rule of Dorgelo (1925) and of Ornstein & Burger (1926) requires that $S_1/S_2 = g_1/g_2$ for the s-resolved hfs componets of either D line, where $S_1 = S(1, 1) + S(1, 2)$ and $S_2 = S(2, 1) + S(2, 2)$. If small wavelength differences are ignored once more, the relevant equality $f_1 \sim f_2$ derived above can be obtained more easily in this way. This sum rule follows from the fundamental, general expressions for the line strengths within an L-S coupling multiplet, which yield the detailed ratios given by Condon & Shortley for many multiplets, including some for which the sum rule by itself is insufficient to specify even the relative strengths of all of the hfs lines.

This simple result that $f_1 = f_2 \sim f$ for the two s-resolved hfs components of either D line also applies separately to each of the resonance doublet lines of both ^{7}Li I and K I, because those atoms have the same level structures and quantum numbers as Na I. Some pertinent data for the various pairs of hfs components are collected in Table 4. In column (5), the splitting of each pair of s-resolved hfs components is expressed in velocity units.

TABLE 4

HYPERFINE STRUCTURE COMPONENTS

Atom	J -> J'	F -> F'	λ_{air} (Å)	Δv (km s^{-1})	f	$gf/(g_1+g_2)$
^{7}Li I	1/2 -> 3/2	1 -> 0,1,2	6707.754	0.537	0.4946	0.1855
		2 -> 1,2,3	6707.766		0.4946	0.3091
	1/2 -> 1/2	1 -> 1,2	6707.905	0.537	0.2473	0.0927
		2 -> 1,2	6707.917		0.2473	0.1546
Na I	1/2 -> 3/2	1 -> 0,1,2	5889.9386	1.01	0.6311	0.2367
		2 -> 1,2,3	5889.9584		0.6311	0.3944
	1/2 -> 1/2	1 -> 1,2	5895.9108	1.08	0.3180	0.11925
		2 -> 1,2	5895.9321		0.3180	0.19875
Na I	1/2 -> 3/2	1 -> 0,1,2	3302.364	0.590	0.00897	0.00336
		2 -> 1,2,3	3302.3705		0.00897	0.00561
	1/2 -> 1/2	1 -> 1,2	3302.974	0.590	0.00448	0.00168
		2 -> 1,2	3302.9805		0.00448	0.00280
K I	1/2 -> 3/2	1 -> 0,1,2	7664.906	0.352	0.6816	0.2556
		2 -> 1,2,3	7664.915		0.6816	0.4260
	1/2 -> 1/2	1 -> 1,2	7698.969	0.351	0.3393	0.1272
		2 -> 1,2	7698.978		0.3393	0.2121

APPENDIX B

The theoretical line profiles were calculated in the following way. The residual intensity r_λ in the region of an absorption line arising in an individual interstellar cloud is

$$r_\lambda = e^{-\tau_\lambda}, \tag{B1}$$

and the optical depth is given by

$$\tau_\lambda = \int_a^b [n_1(z)a_{1\lambda}(z) + n_2(z)a_{2\lambda}(z)]dz \sim a_{1\lambda}N_1 + a_{2\lambda}N_2, \tag{B2}$$

where the two s-resolved hfs components discussed in Appendix A are taken into account explicitly, and the absorption coefficents $a_{i\lambda}$ are crudely assumed to be independent of position within the cloud. To obtain expressions for the two absorption coefficients, a Maxwellian distribution of radial velocity components of the absorbing atoms was assumed,

$$\Psi(v) = \frac{1}{\sqrt{\pi}\,b} \exp\,[-(v - v_0)^2/b^2], \tag{B3}$$

where b describes the velocity dispersion within the interstellar cloud and v_0 is its radial velocity. The total absorption coefficient is then given by (Hobbs 1969b)

$$a_\lambda = \tau_\lambda/N = a_0\left\{\frac{g_1 f_1}{g_1+g_2}\exp\left[-\left(\frac{\lambda_0}{\lambda_1}\right)^2\left(x+\frac{\alpha}{2}\right)^2\right] + \frac{g_2 f_2}{g_1+g_2}\exp\left[-\left(\frac{\lambda_0}{\lambda_2}\right)^2\left(x-\frac{\alpha}{2}\right)^2\right]\right\}, \tag{B4}$$

where the total column density $N \sim N_1 + N_2$, and the $F = 1, 2$ hfs levels of the ground $^2S_{1/2}$ level are assumed to be statistically populated,

$$\frac{N_1}{N} \sim \frac{N_1}{N_1+N_2} \sim \frac{g_1}{g_1+g_2} \quad \text{and} \quad \frac{N_2}{N} \sim \frac{N_2}{N_1+N_2} \sim \frac{g_2}{g_1+g_2}.$$

The value $v_0 = 0$ has been temporarily adopted here, for simplicity of notation. The variable $x = (c/b)(\lambda - \lambda_0)/\lambda_0$ gives the wavelength in dimensionless units, where $\lambda_0 = (\lambda_1 + \lambda_2)/2$ is an appropriate reference wavelength and λ_1 and λ_2 are the laboratory wavelengths of the two s-resolved hfs line components. The quantity $\alpha = (c/b)(\lambda_2 - \lambda_1)/\lambda_0$ is a dimensionless measure of the hfs splitting. The normalization of the absorption coefficient,

$$a_0 \sim \frac{\sqrt{\pi}\,e^2}{m_e v_0}\frac{1}{b} \tag{B5}$$

is fixed by the connection between the oscillator strength and the integral of the absorption coefficient over either s-resolved hfs line component,

$$\int_0^\infty a_0 \exp\left[-\left(\frac{\lambda_0}{\lambda_1}\right)^2\left(x+\frac{\alpha}{2}\right)^2\right]dx \sim \int_0^\infty a_0 \exp\left[-\left(\frac{\lambda_0}{\lambda_2}\right)^2\left(x-\frac{\alpha}{2}\right)^2\right]dx \sim \frac{\pi e^2}{m_e v_0^2}.$$

The unresolved limit must be recovered in equation (B4) by setting $\alpha = 0$, and hence $\lambda_1 = \lambda_2 = \lambda_0$. This limit therefore requires that $f_1 = f_2 = f$, where $f = 0.318$ is the oscillator strength of the unresolved D_1 line, a result which was deduced independently from atomic theory in Appendix A. With $g_1 = 3$, $g_2 = 5$, and $f_1 = f_2 = f$, the final, working expression for the optical depth becomes

$$\tau_\lambda = Nfa_0\left\{\frac{3}{8}\exp\left[-\left(\frac{\lambda_0}{\lambda_1}\right)^2\left(x+\frac{\alpha}{2}\right)^2\right]+\frac{5}{8}\exp\left[-\left(\frac{\lambda_0}{\lambda_2}\right)^2\left(x-\frac{\alpha}{2}\right)^2\right]\right\}. \quad \text{(B6)}$$

The wavelength ratios which appear in the exponentials can usually be ignored in practice, since $(\lambda_0/\lambda_1) \sim (\lambda_2/\lambda_0) \sim 1 + (2 \times 10^{-6})$ for the D_1 line. For any choice of the three free parameters N, b, and (in general) v_0 which characterize an absorbing cloud, the intrinsic line profile was calculated from equations (B6), (B5), and (B1). For comparison with the observations, this intrinsic profile was further convolved with the instrumental profile described in the main text, in order to obtain the observable line profile.

REFERENCES

Barlow, M. J., Crawford, I. A., Diego, F., Dryburgh, M., Fish, A. C., Howarth, I. D., Spyromilio, J., & Walker, D. D. 1994, MNRAS, submitted
Bertin, P., Lallement, R., Ferlet, R., & Vidal-Madjar, A. 1993, A&A, 278, 549
Black, J. H., & van Dishoeck, E. F. 1988, ApJ, 331, 986
———. 1991, ApJ, 369, L9
Blades, J. C., Wynne-Jones, I., & Wayte, R. C. 1980, MNRAS, 193, 849
Bohlin, R. C., Hill, J., Jenkins, E. B., Savage, B. D., Snow, T. P., Spitzer, L., & York, D. G. 1983, ApJS, 51, 277
Centurion, M., & Vladilo, G. 1991, ApJ, 372, 494
Condon, E. U., & Shortley, G. H. 1963, The Theory of Atomic Spectra (Cambridge: Univ. Cambridge Press)
Cowan, R. D. 1981, The Theory of Atomic Structure and Spectra (Berkeley: Univ. California Press)
Crawford, I. A. 1991, A&A, 247, 183
———. 1992, MNRAS, 259, 47
Crawford, I. A., Barlow, M. J., Diego, F., & Spyromilio, J. 1994, MNRAS, 266, 903
Crutcher, R. M. 1975, ApJ, 202, 634
Dickey, J. M., Salpeter, E. E., & Terzian, Y. 1978, ApJS, 36, 77
Diplas, A., & Savage, B. D. 1994, ApJS, in press
Dorgelo, H. B. 1925, Phys. Zs., 26, 756
Falgarone, E., & Lequeux, J. 1973, A&A, 25, 253
Ferlet, R., Vidal-Madjar, A., & Gry, C. 1985, ApJ, 298, 838
Ferlet, R., Vidal-Madjar, A., Laurent, C., & York, D. G. 1980, ApJ, 242, 576
Fowler, J. R. 1994, in preparation
Frisch, P. C. 1981, Nature, 293, 377
Frisch, P. C., & York, D. G. 1984, in IAU Colloq. 81, Local Interstellar Medium, ed. Y. Kondo, F. C. Bruhweiler, & B. D. Savage (NASA CP-2345), 113
Frisch, P. C., York, D. G., & Fowler, J. R. 1987, ApJ, 320, 842
Fuller, G. A., & Myers, P. C. 1993, ApJ, 418, 273
Gerstenkorn, S., & Luc, P. 1978, Atlas du spectre d'absorption de la molecule de l'iode entre 14,800–20,000 cm^{-1} (Paris: Ed. C.N.R.S.)
———. 1979, Rev. de Phys. Appliquee, 14, 791
———. 1985, J. de Phys., 46, 867
Gredel, R., van Dishoeck, E. F., & Black, J. H. 1991, ApJ, 251, 625
Heiles, C., & Kulkarni, S. R. 1987, in Physical Processes in Interstellar Clouds, ed. G. E. Morfill & M. Scholer (Dordrecht: Reidel), 13
Hobbs, L. M. 1969a, ApJ, 157, 135
———. 1969b, ApJ, 157, 165
———. 1974a, ApJ, 191, 381
———. 1974b, ApJ, 191, 395
———. 1976, ApJ, 203, 143
———. 1978a, ApJ, 222, 491
———. 1978b, ApJS, 38, 129
Hobbs, L. M., Blitz, L., & Magnani, L. 1986, ApJ, 306, L109
Hobbs, L. M., & Welty, D. E. 1991, ApJ, 368, 426 (Paper I)
Jenkins, E. B. 1986, ApJ, 304, 739
Jenkins, E. B., Lees, J. F., van Dishoeck, E. F., & Wilcots, E. M. 1989, ApJ, 343, 785
Jenkins, E. B., Savage, B. D., & Spitzer, L. 1986, ApJ, 301, 355
Jeys, T. H. 1991, Lincoln Lab. J., 4, no. 2, 133
Joseph, C. L., & Jenkins, E. B. 1991, ApJ, 368, 201
Kroll, M., & Innes, K. K. 1970, J. Mol. Spectrosc., 36, 295
Lambert, D. L., Sheffer, Y., & Crane, P. 1990, ApJ, 359, L19
Lauroesch, J. T., Hobbs, L. M., Morton, D. C., Spitzer, L., Welty, D. E., & York, D. G. 1994, in preparation
Liszt, H. S. 1983, ApJ, 275, 163
Magnani, L., Blitz, L., & Mundy, L. 1985, ApJ, 295, 402
Marschall, L., & Hobbs, L. M. 1973, ApJ, 173, 43
Martin, E. R. 1981, Ph.D. dissertation, Princeton Univ.
Martin, E. R., & York, D. G. 1982, ApJ, 257, 135
McNutt, D. P., & Mack, J. E. 1963, J. Geophys. Res., 68, 3419
Megie, G., Bos, F., Blamont, J. E., & Chanin, M. L. 1978, Planet. Space Sci, 26, 27
Meyer, D. M., & Roth, K. C. 1991, ApJ, 376, L49
Meyers, K. A., Snow, T. P., Federman, S. R., & Breger, M. 1985, ApJ, 288, 148
Morton, D. C. 1991, ApJS, 77, 119
Myers, P. C. 1983, ApJ, 270, 105
Ornstein, L. S., & Burger, H. C. 1926, Zs. f. Phys., 40, 403
Payne, H. E., Salpeter, E. E., & Terzian, Y. 1983, ApJ, 272, 540
Peters, G. E. 1988, Be Star Newsletter 19
Pettini, M. 1988, Proc. Astr. Soc. Australia, 7, 527
Pound, M. W., Bania, T. M., & Wilson, R. W. 1990, ApJ, 351, 165
Sansonetti, C. J. 1987, private communication
Savage, B. D., Bohlin, R. C., Drake, J. F., & Budich, W. 1977, ApJ, 216, 291
Savage, B. D., Cardelli, J. A., & Sofia, U. J. 1992, ApJ, 401, 706
Scalo, J. 1990, in Physical Processes in Fragmentation and Star Formation, ed. R. Capuzzo-Dolcetta, C. Chiosi, & A. Di Fazio (Dordrecht: Kluwer), 151
Shull, J. M., & Van Steenberg, M. E. 1985, ApJ, 294, 599
Snow, T. P., & Meyers, K. A. 1979, ApJ, 229, 545
Snowden, S. L., McCammon, D., & Verter, F. 1993, ApJ, 409, L21
Spitzer, L. 1968, in Stars and Stellar Systems, Vol. 7, Nebulae and Interstellar Matter, ed. B. M. Middlehurst & L. H. Aller (Chicago: Univ. Chicago Press), 1
———. 1978, Physical Processes in the Interstellar Medium (New York: Wiley)
Spitzer, L., & Fitzpatrick, E. L. 1993, ApJ, 409, 299
Stokes, G. M. 1978, ApJS, 36, 115
Tull, R. G. 1972, in Proc. ESO/CERN Conference on Auxiliary Instrumentation for Large Telescopes (Geneva: ESO), 259
Vallerga, J. V., Vedder, P. W., Craig, N., & Welsh, B. Y. 1993, ApJ, 411, 729
Welsh, B. Y., Vedder, P. W., & Vallerga, J. V. 1990, ApJ, 358, 473
Welsh, B. Y., Vedder, P. W., Vallerga, J. V., & Craig, N. 1991, ApJ, 381, 462
Welty, D. E., Hobbs, L. M., & York, D. G. 1991, ApJS, 75, 425
Welty, D. E., Hobbs, L. M., Lauroesch, J. T., Morton, D. C., Spitzer, L., & York, D. G. 1994a, in preparation
Welty, D. E., Morton, D. C., & Hobbs, L. M. 1994b, in preparation
White, R. E., & Bally, J. 1993, ApJ, 409, 234
Willmarth, D. 1994, private communication
York, D. G., Spitzer, L., Bohlin, R. C., Hill, J., Jenkins, E. B., Savage, B. D., & Snow, T. P. 1983, ApJ, 266, L55
Zimmermann, T., & Ungerechts, H. 1990, A&A, 238, 337